Speleothem-Based Hydroclimate Reconstruction of Northeastern Mexico Across the Last Deglaciation

by

Aviva B. Intveld

Submitted to the Department of Earth, Atmospheric, and Planetary Sciences
in partial fulfillment of the requirements for the degree of

Bachelor of Science in Earth, Atmospheric, and Planetary Sciences

at the

MASSACHUSETTS INSTITUTE OF TECHNOLOGY

May 2023

Author .....
Department of Earth, Atmospheric, and Planetary Sciences
May 19, 2023

Certified by .....
David McGee
Associate Professor
Thesis Supervisor

Accepted by .....
Thomas A. Herring
Chair, Committee on Undergraduate Program

Speleothem-Based Hydroclimate Reconstruction of Northeastern Mexico Across the Last Deglaciation

by

Aviva B. Intveld

Submitted to the Department of Earth, Atmospheric, and Planetary Sciences
on May 19, 2023, in partial fulfillment of the
requirements for the degree of
Bachelor of Science in Earth, Atmospheric, and Planetary Sciences

Abstract

As anthropogenic global warming intensifies, climate models predict more frequent drought conditions across Northeastern Mexico, but regional paleoclimate data is necessary to inform the spatial extent and severity of these droughts. In this thesis, we present a centennial-scale resolution record of Northeastern Mexico hydroclimate spanning 21.77 to 11.56 ka using a speleothem from Rioverde, San Luis Potosí, Mexico. We use trace element ratio data to reconstruct local water balance (P - ET) and compare our results to neighboring proxies and climate models to investigate regional coherency and climate forcings. Our record captures wet conditions during the Last Glacial Maximum, dry conditions during Heinrich Stadial 1, and wet conditions during the Bolling-Allerod Warming, with implications for defining glacial climate and assessing the Mesoamerican North-South precipitation dipole on millennial to orbital timescales. Our results also demonstrate a dynamic control on precipitation via changes in the Atlantic-Pacific SST gradient. Furthermore, our results help fill a crucial gap in our knowledge of the climatic background of the First Peopling of the Americas and offer a potential route for the Peopling of Mexico between 15.5 and 13 ka. Ultimately, this work provides a precisely dated and high-resolution record in an understudied region to better predict future climate and reconstruct human history.

Thesis Supervisor: David McGee
Title: Associate Professor

Acknowledgments

First, thank you to David McGee, who has gifted me with four years of mentorship, wisdom, and warmth. Thank you for your instruction in ICP training, your insight during data analysis and interpretation, your talent for balancing the big picture vision with an attention to detail, and the endless sessions of just trying to make sense of it all. Both this thesis and I have benefited from your regular guidance and advice at every stage.

Thank you to the entire McGee Lab: Ben Tiger, Madi Wittmer, Cameron Batchelor, and Adam Jost. You have each contributed so much, from code and modeling support to lessons in climate dynamics and writing advice. Thank you also to Christopher Kinsley, who welcomed me to the lab and to Mexican Paleoclimate in Fall 2021.

Thank you to: our collaborators Kathleen Johnson at UC Irvine and Sergio Sanchez-Armass from the Asociación Potosina de Montañismo y Espeleología (APME), who provided expertise in karst dynamics and local geology; Priyadarsi Roy at the Universidad Nacional Autonoma de Mexico for sharing the raw data from his work; Suzanne Ankerstjerne at Iowa State for stable isotope analysis; and Gabi Serrato Marks, whose doctoral thesis provided the basis for this work.

Thank you to the MIT Climate and Sustainability Consortium for inspiration, funding, and communication instruction; to Jane Abbott for counsel and encouragement; and to my peers in EAPS for community and solidarity.

Finally, I am especially grateful to my parents and my friends. Thank you for your love.

"All care [...] has a tacit, if open-ended, relationship to futurity: you feed someone so that she will not grow malnourished; you treat a wound so that it will not become infected; you water seeds in hopes that they will grow. It's not that there is no present in care. [...] It's more that, in caring, time is folded: one is attending to the effects of past actions, attempting to mitigate present suffering, and doing what one can to reduce or obviate future suffering, all at once."

-Maggie Nelson, *On Freedom*

Contents

Chapter 1

Introduction

1.1 Northeastern Mexico – An Overview

Located in the middle of Mexico's arid zone, Northeastern Mexico is particularly vulnerable to the effects of drought. The region currently relies on limited and over-exploited groundwater aquifers to supply over 60% of its potable water, while water stress values rank between 20 and 86 percent, measured as the ratio of annual water withdrawals to annual renewable freshwater supply (Martinez et al. 2009). At the same time, Northeastern Mexico is experiencing one of the highest urban population growth rates in the country, and as anthropogenic global warming intensifies, climate models predict more frequent droughts and the expansion of drylands in the subtropics (Seager et al. 2013; Rauscher et al. 2010). As stressors increase on the already depleted aquifers, water scarcity emerges as a preeminent challenge. Understanding regional hydroclimate and its response to climate extremes is therefore paramount to safeguarding this landscape and its communities.

Model predictions of the response of Northeastern Mexico to future warming utilize instrumental data and the historic record. However, both datasets are limited in time, which precludes our investigation into how the magnitude of recent or predicted near-future drying compares to natural climate variability (Bhattacharya et al. 2020).Therefore, in order to accurately predict how the region will respond to future warming, a crucial approach is to look through recent geologic time (last 22,000

years) to past responses in local water balance.

Reconstructing terrestrial hydroclimate of the past relies on a variety of climate proxy records, most notably lake sediment cores and cave sediments, or speleothems. While lake sediments have limitations in dating accuracy and material availability, speleothems make excellent paleoclimate archives due to their potential for high-precision Uranium-Thorium dating, their large amount of sample material availability for replication, validation, and temporal resolution, and their sensitivity to climate variability (Griffiths et al. 2010). However, in Northeastern Mexico, proxy records are sparse: to date, only two speleothem-based analyses and three lake sediment-based analyses have been published (Wright et al. 2022; Serrato Marks et al. 2020; Roy et al. 2016; Roy et al. 2019; Roy et al. 2020). This record paucity prevents a detailed investigation into the climate response and climate drivers of Northeastern Mexico.

Furthermore, while more than half of Mexico classifies as an arid or semi-arid climate (Schmidt 1989), regional hydroclimate can vary at small spatial scales. Beyond precipitation amount, additional factors such as topography, vegetation, soil cover, bedrock, and elevation can all impact local water balance. For this reason, increasing the spatial resolution of proxy records is necessary not only for regional comparison but for informed decision-making at the local level. This thesis presents a new late Pleistocene - early Holocene speleothem proxy record with centennial resolution from understudied Northeastern Mexico, filling a critical spatial and temporal gap and contributing to our understanding of past regional climate variability and climate drivers.

1.2 San Luis Potosí – Site Significance

While crucial for informing accurate climate predictions, paleoclimate reconstructions of the late Pleistocene - early Holocene also play a significant role in establishing a climatic background for early human evolution, tradition, and movement. In particular, San Luis Potosí in Northeastern Mexico, the study site presented in this thesis, sits at a pivotal location in the history of the first peopling of the Americas. Located

near the Atlantic coast of Mexico but still at a high elevation inland, the study site can provide a climatic context to the nearby Mesoamerican archaeological sites of the late Pleistocene - early Holocene as well as help assess the two prevailing first peopling hypotheses.

Despite much research since the late 19th century, the exact timing, route, and motivating factors behind the first peopling of the Americas remains uncertain. In 2021, a new study by Bennett et al. challenged previous research (Llamas et al. 2016; Meltzer 2003) by claiming human presence in North America between 21-23 ka, over 5 ka earlier than the prior earliest uncontested date. The results were questioned on the basis of uncertainties in the radiocarbon dating, but their ages are supported by additional sites at Chiquihuite Cave in central Mexico, which found (strongly contested) ages of 31 ka, and Monte Verde in Chile, where stone artifacts, faunal remains, and burned areas suggest (widely accepted) ages between 18.5 and 14.5 ka BP (Ardelean et al. 2020; Dillehay et al. 2015). These two pre-Clovis sites and others challenge the original Clovis Ice-Free Corridor hypothesis, in which Siberian hunter-gatherers (Clovis peoples) are thought to have first reached the Americas via the exposed "Ice Free" Beringia land bridge approximately 11.5 ka BP (Waters et al. 2007).

The "Kelp Highway," an alternative to the Clovis-first theory, is one answer to these older dates. The Kelp Highway proposes that early humans migrated over 10,000 km by boat along the Pacific Rim from Northeast Asia to the western coasts of North and South America, utilizing kelp forests for productive fishing, holdfasts, and reduced wave energy (Erlandson et al. 2007). This coastal migration theory could offer a path to America as early as 16 ka BP. Finally, an additional (more contested) theory suggests that humans entered the Americas even earlier around 26 ka BP, before the peak of the Last Glacial Maximum, when there would have been a navigable land route from Asia to North America (Bennett et al. 2021).

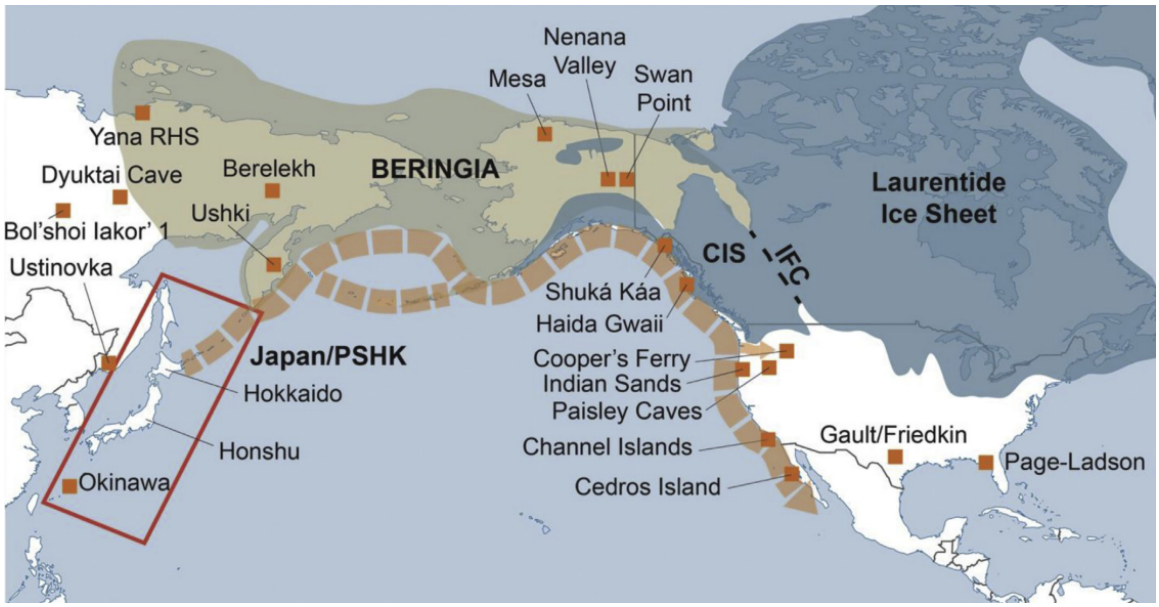

Figure 1-1: The two proposed routes for the First Peopling of the Americas. The "Ice Free Corridor" route is noted via a dashed black line whereas the "Kelp Highway" route is noted via a dashed orange arrow. Paleolithic archaeological sites are noted with orange squares. In the modern-day United States, inland routes branch off from the southward coastal migration (Figure from Davis et al. 2020).

The inherent interdisciplinary nature of this question is one of the major difficulties in establishing a chronology for the first peopling of the Americas. A robust timeline requires the synthesis of three disparate camps of data: 1) First people archaeological sites which display a clear association between unambiguous artifacts (projectile points, blades) and accurate dating, 2) Genetic evidence of ancient mitochondrial DNA sequenced from pre-Columbian skeletons, and 3) Local and regional paleoclimate and paleoenvironment reconstructions to provide insight into habitable windows in space and time. Each of these camps face their own discussions and controversies, compounding uncertainty. Integrating the chronological records of each three camps while accounting for their limitations is beyond the scope of this thesis, though this work can provide critical insight into early human movement and habitable inland zones by identifying periods of localized drought and periods of relatively higher water availability.

Through a proxy data analysis of the late Pleistocene - early Holocene speleothem record presented in this thesis, alongside a comparison of other local proxies, we

can help inform the field's understanding of past environmental changes which may have influenced human migration during the Last Glacial Maximum and introduce a paleoclimatic argument into a question that has long been approached largely via the disciplines of archaeology and genetics alone.

1.3 Northeast Mexico Climate Controls

Interpreting the climate signal of a paleoclimate proxy record first requires a detailed understanding of local climate and modern climate drivers. Today, the climatology of Northeastern Mexico is characterized by wet-hot summers and cool-dry winters. Approximately 55% of all precipitation in the region occurs during Boreal summer, between June and August; fall precipitation makes up another 30%; and spring and winter account for 10% and 5%, respectively (source: weatherbase.com). The sources of each seasonal precipitation amount vary: small contributions in winter and spring are related to variations in the El Niño Southern Oscillation (ENSO) and tropical Atlantic meridional gradient variability (Wang et al. 2006; Roy et al. 2016), and autumn precipitation is linked to increased tropical cyclone and hurricane activity (Roy et al. 2015, 2019, 2020). Summer precipitation, the dominant contributor to annual rainfall, is associated with moisture transport from the Caribbean Sea and Gulf of Mexico via the northward branch of the Caribbean Low Level Jet (CLLJ) (Roy et al. 2016).

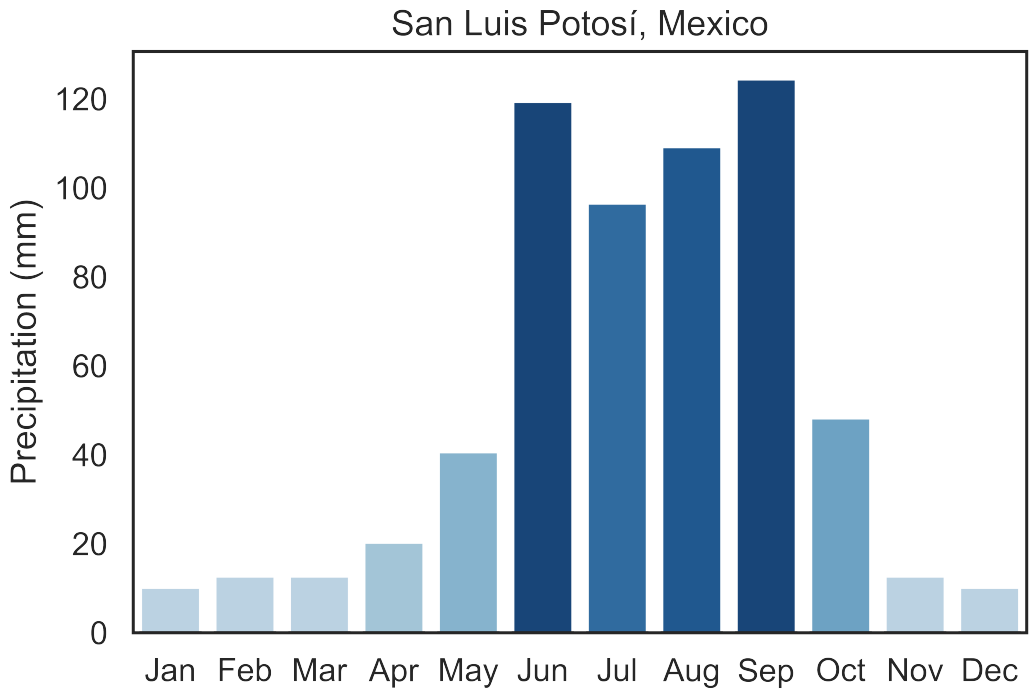

Figure 1-2: El Potosí Basin is located in NE Mexico west of the Sierra Madre Oriental Mountains. Modern precipitation data (source: weatherbase.com) from San José Gallinas, San Luis Potosi (22º01"N, 100º12"W, 764.1 m elevation, 78 km south of Grutas de la Catedral) is shown averaged over the past 60 years. The data shows the early summer moisture peak in June via the CLLJ, the mid-summer dry spell, and the contribution of autumn moisture via tropical cyclones (Roy et al. 2016).

Because the sources and dynamics of precipitation over Northeastern Mexico vary seasonally, and as the proxy data resolution of the record presented in this work is on the scale of 90 years (See Section 3.2), our discussion of climate controls on NE Mexico precipitation will focus on multi-decadal to millennial timescales. At this temporal resolution, existing paleoclimate studies have largely explored two climate controls: thermodynamic forcings, which modulate the total column water vapor volume via changes in Caribbean SSTs, and dynamic forcings, which modulate the strength and position of the CLLJ via orbital shifts in insolation, shifts in the North-South location of the trade winds convergence belt, and shifting Atlantic-Pacific SST gradients (Wright et al. 2022; Roy et al. 2016; Bhattacharya et al. 2020). The following section will discuss controls on both the CLLJ and SSTs and offer a brief

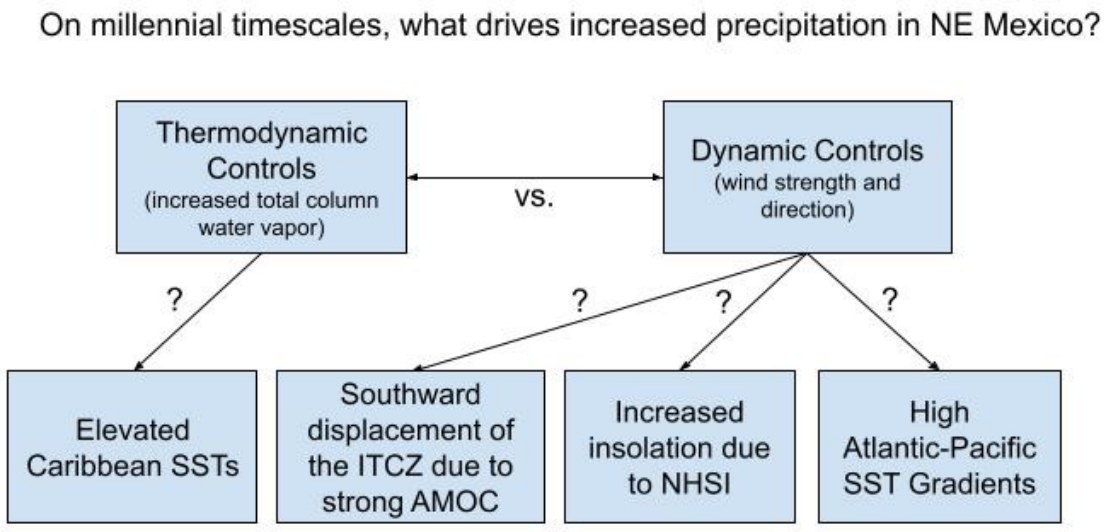

Figure 1-3: A diagram of possible drivers of increased precipitation over Northeastern Mexico on millennial timescales, separated into thermodynamic controls and dynamic controls. Contested correlations are indicated with a question mark and discussed further in the text.

review of the existing literature on implications for precipitation in Northeastern Mexico, to be further explored in Section 4.1.

First, the CLLJ, an easterly zonal wind over the Caribbean Sea, is the primary mechanism by which moisture is transported from the Atlantic Ocean to the Atlantic slope of Northern Mexico (Wright et al. 2022). While the strong low-level wind flow of the CLLJ is present year-round, observations show semi-annual variations, with two maxima in the summer (July) and winter (February) at approximately 925 hPa and two minima in the fall and spring (Wang 2007; Maldonado et al. 2015). Previous studies have found that the two CLLJ maxima differ in origin, physical mechanisms, and impact on Central American precipitation patterns: in Northern Mexico, only the Boreal summer maximum (June through August) is associated with increased moisture flux and precipitation in the modern day (Wright et al. 2022). This suggests that changes in precipitation linked to variability in the CLLJ strength imply a dominance of summer precipitation in the proxy record.

In the modern, the strengthening summer CLLJ is associated with a sea level

pressure maximum over the Caribbean Sea, a tropical cyclogenesis minimum, a brief interruption in precipitation during the CLLJ peak (the mid-summer drought), an an average increase in precipitation over Northern Mexico by an estimated 1-2 mm per day (Wang 2007; Maldonado et al. 2015; Amador 2008). To date, the processes controlling CLLJ strength remain largely unknown, but multiple climate forcings have been explored in connection to CLLJ variability and precipitation over Northern Mexico (Amador 2008).

On seasonal timescales, a strengthening CLLJ has been linked to increasing insolation (solar heating reaching the earth's surface increasing evaporation) and northward migration of the Intertropical Convergence Zone (ITCZ), an equatorial band of trade wind convergence that shifts with the thermal equator (Wright et al. 2022). On longer, orbital time scales, a strengthening CLLJ has been linked to precessional changes (Wright et al. 2022; Buis 2020). Precessional changes track changes in the direction of Earth's spin axis, which rotates on a cycle every 25,771 years, shifting the location of perihelion (the point of closest approach to the sun) between seasons and accentuating seasonal contrasts in one hemisphere. Approximately 12,700 years ago, perihelion occurred during summer in the Northern Hemisphere, accentuating seasonal contrasts in the Northern Hemisphere and thus increasing summer insolation in the Northern Hemisphere – known as the Northern Hemisphere Summer Insolation (NHSI) – ultimately increasing CLLJ strength, as observed during insolation increases during modern-day summer (Roy et al. 2016).

For each of these links, differentiating between correlation and causality can be difficult. Some paleoclimate studies (Roy et al. 2016) argue a connection between an NHSI-driven strong CLLJ and periods of increased precipitation over NE Mexico, but others find a limited role for NHSI and argue that others seasons of insolation are more important drivers of hydroclimate (Roy et al. 2019, 2020). A weakening CLLJ strength has also been linked to the southward movement of the ITCZ driven by a shutdown of the Atlantic Meridional Circulation (AMOC), the strong circulation system that transports heat into the Northern Hemisphere (Roy et al. 2016). On seasonal timescales, however, the southward movement of the ITCZ has been linked

to the strengthening CLLJ during Boreal winter (Cook et al. 2010). While we assume that this record does not dominantly capture the winter precipitation signal, this modern-day observation challenges the connection between ITCZ position and CLLJ strength.

CLLJ dynamics have also been linked to Atlantic-Pacific SST gradients. Results from a multiproxy speleothem record spanning the last millennium as well as an atmospheric general circulation model demonstrate that warmer Atlantic SSTs relative to Pacific SSTs drive extended wet periods in Northeast Mexico (Wright et al. 2022). An additional study using a model simulation trained on multiple proxy types over the last millennium found that a high Atlantic-Pacific pressure gradient is associated with strengthening easterly winds (a strong CLLJ) but also a southward displacement of the ITCZ (Bhattacharya et al. 2020). While these millennial-scale results are promising, they are confined to the Common Era and as such the impact of SST gradients on longer-term hydroclimate patterns is still under review.

Finally, we consider thermodynamic controls on precipitation over Northeast Mexico. Several lake sediment-based hydroclimate reconstruction studies associated warm Gulf of Mexico SSTs with periods of increased tropical storms and hurricanes on millennial time-scales (Roy et al. 2019, 2020). However, a limitation to this work is that increases in climate extremes may not necessarily shift with the mean precipitation captured in the speleothem record presented in this thesis. Wright et al. (2022) also notes thermodynamic controls on NE Mexican precipitation on orbital timescales, with speleothem δ18O exhibiting high correlation with regional SSTs, including the Tropical North Atlantic, the Gulf of Mexico, the Caribbean Sea, and the Eastern Equatorial Pacific.

Both thermodynamic and dynamic controls may work in tandem: elevated Caribbean SSTs, for example, would both increase atmospheric water vapor thermodynamically and also increase the Atlantic-Pacific temperature gradient, decreasing CLLJ strength and amplifying a wet Northeastern Mexico signal. While we assume that the proxy record reflects the impact of both, the aim of this thesis will be to explore which of the two forcings dominate on millennial timescales, and how the dominant forcing

compares to nearby records.

1.4 Karst Hydrology and Chemistry

Interpreting the speleothem proxy record also requires a foundational understanding in how climate signals are recorded in cave sediments and what processes impact those signals. The following section will provide a brief overview into speleothem forming processes and how they inform proxy interpretation.

Karst Hydrology

Calcareous speleothems form when meteoric water falling onto the karst landscape infiltrates the overburden above the cave and percolates through the epikarst, entering the cave environment as drip water and precipitating CaCO3 when it drops onto the cave floor. In this way, stalagmites (used here interchangeably with the term speleothem) capture chemical signatures of precipitation as they grow upwards over time.

Proxies for Hydroclimate

There are a variety of useful proxies associated with the chemical composition of stalagmites that can be employed to analyze changes in past hydroclimate, but this thesis will focus specifically on δ18O, δ13C, and ratios of Mg and Sr to Ca.

First, in areas in the tropics (such as the study site presented in this work), semi-arid areas, and areas dominated by strong convective monsoonal climates, δ18O records are dominated by the amount effect, in which more negative (depleted) δ18O precipitation values indicate increased rainfall amount, and more positive (enriched) δ18O precipitation values indicate decreased rainfall amount (Fairchild et al. 2007). While this relationship is widely observed on timescales from seasonal to decadal to centennial to millennial, it assumes that the δ18O values of calcite reflect those of precipitation above the cave site, which in turn reflect a relatively constant ocean

isotopic composition. This relationship may be complicated by karst processes, as fractionation in the karst and cave as well as bias towards seasons with more groundwater recharge can cause speleothem δ18O to not directly track δ18O of precipitation above the cave (Baker et al. 2019). As a result, the δ18O record cannot always be directly interpreted as rainfall amount (see Section 3.2 for more).

Second, variations in the δ13C record can reflect several local processes. The three most common controls resulting in a more negative (positive) δ13C signal include a higher (lower) C3 to C4 ratio in vegetation above the cave, a higher (lower) amount of organic matter respiration above the cave, and a lower (higher) amount of degassing in the vadose zone as a result of stronger (weaker) infiltration of water (Fairchild et al. 2006). Disentangling the imprint of each of these processes can be difficult and requires a multiproxy approach involving lake pollen records to reconstruct C3/C4 ratio shifts and vegetative density shifts, and tracking δ13C covariation with trace element ratios (see Section 3.3 for more).

Finally, though less-frequently utilized, trace element ratios such as Mg/Ca and Sr/Ca can reflect climate-dependent karst-water processes (Cruz et al. 2007). In particular, studies from different environments around the world have found that when Mg/Ca and Sr/Ca co-vary, their ratios reflect the meteoric water infiltration rate into the vadose zone and thus the amount of local rainfall (Fairchild et al. 2000). Co-variation of Mg/Ca and Sr/Ca occurs as a result of Prior Calcite Precipitation (PCP), which reflects the ability of infiltration waters to degas. When infiltration waters degas, the resulting water exhibits a higher Mg and Sr to Ca ratio. (For further discussion, see below and Section 3.3)

Ultimately, each of these proxies will be utilized in this work to explore variations in hydroclimate in Northeast Mexico across the last deglaciation.

Prior Calcite Precipitation (PCP)

In this section we present a more thorough explanation of Prior Calcite Precipitation, as the paleoclimate reconstruction presented in this thesis relies heavily on this karst process for hydroclimate inferences.

In arid and semi-arid regions such as the study site presented in this work, PCP can be a primary control on dripwater and speleothem trace element chemistry. PCP occurs when infiltration water containing minor and trace elements percolates through the epikarst, degassing dissolved CO2 in pore spaces and fissures and precipitating calcite in the vadose zone (Treble et al. 2015). Upon reaching the cave ceiling, the drip water equilibrates with cave PCO2, which is a function of the concentration of the gaseous CO2 in the cave. Once the fluid equilibrates with the PCO2 conditions in the cave, calcite can precipitate on the cave floor and form a stalagmite. In this way, the degree of this prior precipitation is recorded in the stalagmite.

When analyzing a record on seasonal timescales, the changes in cave PCO2 can have a large impact on the trace element record. Cave PCO2 is controlled by CO2 influx/efflux of the cave. Factors that cause CO2 influx (efflux) include increased (decreased) cave biological activity, increased (decreased) production by microbial and root respiration in overlying soil and vadose zone, and less (more) ventilation in the cave occurring due to a lower (higher) temperature gradient with the cave exterior during (cooler) warmer months (Fairchild et al. 2006). However, on decadal to orbital timescales, these effects are less noted.

Most often, the degree of PCP reflects changes in aridity: the less moisture that enters the cave (e.g. the lower the levels of recharge into the karst aquifer), the less water fills the pore spaces within the karst, and thus the higher the ability of the infiltration waters to degas. As the infiltration waters degas, a higher volume of calcite precipitates in the unsaturated zone in the overlying aquifer or on the cave ceiling. Because Mg and Sr are excluded from calcite relative to Ca during PCP the remaining water has higher Mg/Ca and Sr/Ca ratios, which are then imparted to speleothem calcite when it forms (Day and Henderson, 2013). We will utilize this karst-water process to make hydroclimate climate inferences from our record in Section 4.1.

Chapter 2

Methods

2.1 Sample Collection

Stalagmite GC1 was collected in 2017 from the cave Grutas de la Catedral (GC) by Dr. Gabi Serrato Marks, a former graduate student in the McGee Lab, and members of the San Luis Potosí-based caving group, the Asociación Potosina de Montañismo y Espeleología (APME). GC is the largest cave in a system of caves near Rioverde, San Luis Potosí, Mexico. While the entrance (21°94 "N, 100°24 "W, 2000 m.a.s.l.) is open to tourists, the collection location of GC1 is approximately a 1.5 hour-long hike from the tourist area and is 20 meters down, accessible only via vertical caving equipment. As a result, the chamber is not influenced by tourist presence (Serrato Marks 2020).

At approximately 2000m high in elevation, GC1 is within the pine-oak forest range of the Sierra Madre Orientales (between 1,000-2,500 m in elevation). Regional vegetation includes pinyon pines, weeping pines, red oaks, agave, and cacti. As GC1 is on the drier, west-facing slope of the Sierra Madre Orientales, endemic weeping pines are more common than the pinyon pine and alligator juniper, which are characteristic of the wetter east-facing slopes (Rzedowski 1978). The geology surrounding GC1 is karst dominated, with Mesozoic carbonate reef and platform facies of the El Abra formation covered by a thick soil overburden (Johnson, personal communication, 2023).

Stalagmite GC1 is candlestick-shaped and 29 cm in length. The texture alternates between a more frequent translucent gray and a less frequent porous white. Previous

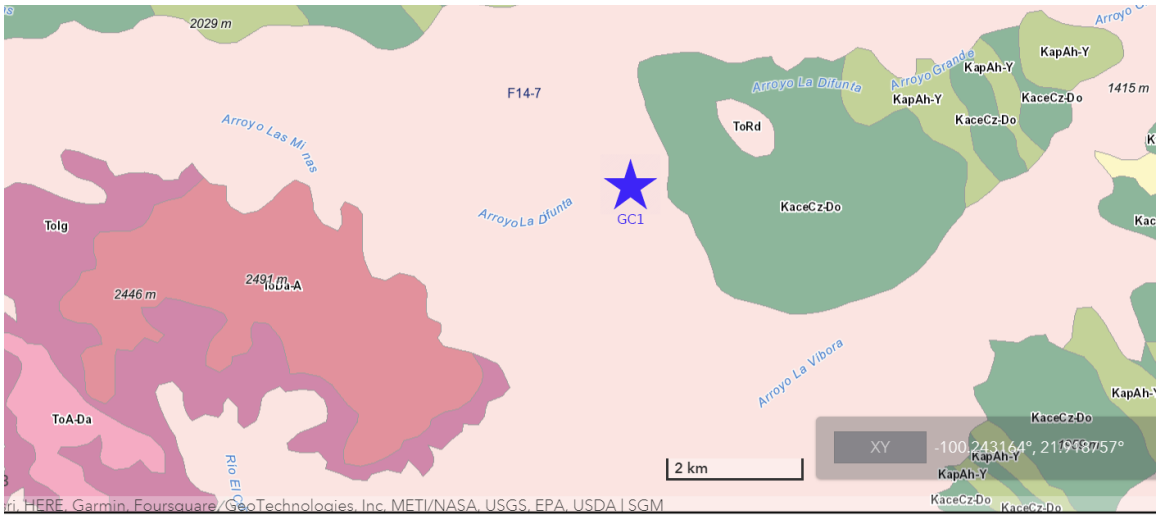

Figure 2-1: A map of the surficial geology surrounding the tourist entrance to GC1 (Lithology scale 1:250,000). Surficial deposits include: Rhyodacite (light pink / ToRd); Mesozoic Limestone-Dolomite of the El Abra Formation (dark green / KaceCz-Do); and Mesozoic Anhydrite-Gypsum (light green / KapAh-Y). The prevalence of limestone-dolomite karst landscapes in NE Mexico makes the region ideal for speleothem growth. (Figure modified from the Government of Mexico Geological Survey)

studies in crystallography demonstrate that aragonite competitively incorporates Sr into its crystal matrix, causing aragonite to be enriched in Sr and depleted in Mg in comparison to calcite (He et al. 2022). As a result, because the trace element ratios do not change based on visible texture within GC1 (see Section 3.2), we assume the sample is wholly calcite rather than aragonite.

At 145 mm from the top, there is a growth hiatus (2 mm in thickness) visible by a thick band of detritus material. The hiatus may have occurred due to a shift in karstic plumbing (e.g. variations in water flow paths), an extended period of below-average rainfall leading to a temporary cessation of dripping, or speleothem erosion (Fairchild & McMillan 2007).

2.2 U-Series Dating

U-Series dating of GC1 was completed between 2017 and 2020 by Dr. Serrato Marks. Dr. Marks dated 18 discrete horizons along the growth axis of the stalagmite, with

a top depth at 11 mm (from the top) and a bottom depth at 270 mm (from the top). Once corrected for contributions of detrital 230Th, these 18 ages span 7.19 ± 0.10 (top) to 21.77 ± 0.19 (bottom) ka before present (BP), with a median age uncertainty of 70 years (±2 standard deviation). An additional horizon at the bottom of the stalagmite was run in a mixed batch and produced a date of 21.4 ± 0.27 ka. As this date is out of stratigraphic order, and as dates of mixed batches (varying ages and U concentrations) are thought to be less trustworthy than unmixed batches, the bottom date was removed from analysis in this thesis.

The growth hiatus started after 11.56 ka and extended until just before 8.84 ka. The younger, upper section of the stalagmite spans 7.19 ± 0.10 to 8.84 ± 0.04 ka BP is constrained by 8 U-series samples. This section was analyzed by Dr. Serrato Marks in relation to the 8.2 ka event for Chapter 4 of her doctoral thesis. The older, bottom half of GC1 spans 11.56 ± 0.14 to 21.77 ± 0.19 ka BP (145 to 270 mm) and is constrained by 10 discrete U-series samples with a mean uncertainty of 325 years. This older section was not analyzed, and underwent only preliminary trace element measurement at very low resolution and no stable isotope measurement. For this thesis, we will analyze the older half of GC1, which captures the end of the last glacial period, Heinrich-Stadial 1, the Bolling-Allerod Warming, and the Younger Dryas Stadial.

2.3 Trace Element Measurements

In order to complete a high-resolution proxy record of GC1 from 11.56 to 21.77 ka BP, we selected samples at approximately 1 mm resolution from 192 to 270 mm (sample vials #384-540, n=77) for trace element (TE) measurement (Ca, Mg, Sr, U). Samples had been previously milled and were chosen based on available remaining powder, as 0.5 mg of powder is necessary for TE measurement due to mass spectrometer sensitivity. TE measurements from 145 to 192 mm (sample vials #290-384, n=47) were completed in 2020 by Dr. Serrato Marks.

Powders were weighed out into samples of approximately 0.5 mg and dissolved in

1 mL 3% ICP solution (0.5 M HNO3). In order to correct for drift during measurement, replicates from CP2, a stalagmite of similar matrix composition to GC1, were prepared in the same fashion (0.5 mg of powder dissolved in 3% nitric acid). In order to check for machine drift between 2017-2020 and present day, 10 samples from 145 to 192 mm were chosen adjacent to the depths Dr. Serrato Marks had analyzed and also prepared in the same fashion. Standards of varying concentrations of Mg, Ca, Sr, Th and U) were prepared by weighing both the amount of standard solution and 3% nitric acid solution before calculating the concentration of each element in the standard so as to account for any offset in pipetting.

Ca, Mg, Sr, U and Th were measured at MIT using the Agilent 7900 ICP-MS in No-Gas mode. Samples were interspersed with one CP2 replicate and one 50% standard every 8 samples. Mg, Sr, and U were scaled to metal/Ca and converted to mmol/mol. Elemental counts per second (CPS) were tracked to ensure concentrations were within detection limits and the calibration curve and well above instrumental blank levels, and Th concentrations were measured as a tracer of aluminosilicate detritus.

Finally, reproducibility metrics were calculated to check for machine drift during the run and machine drift over time. For the 10 CP2 replicates interspersed every 8 samples, the relative standard deviation (RSD) for Mg/Ca was 1.3% and the RSD for Sr/Ca was 0.4%. For the 10 replicate standards interspersed every 8 samples, the RSD for Mg/Ca was 0.9% and the RSD for Sr/Ca was 0.8%. These substantially low RSD values suggest little to no machine drift throughout the runs. For the 10 adjacent samples from 145 to 192 mm, there was no consistent offset between the two datasets, and so the data appears intercomparable, with little to no machine drift between the 2017-2020 measurements and those performed for this thesis.

2.4 Stable Isotope Measurements

From 144.5 to 270 mm, 117 samples containing a minimum of 0.1 mg of powder each (averaging 1 mm depth resolution) were sent for stable isotope analysis to Dr. Suzanne

Ankerstjerne at Iowa State University, Department of Geological and Atmospheric Sciences, Stable Isotope Lab.

Samples were measured via a Thermo Scientific Delta V Plus mass spectrometer in continuous flow mode connected to a Gas Bench with a CombiPAL autosampler. Reference standards (NBS-18, IAEA 603) were used for isotopic corrections, and to assign the data to the appropriate isotopic scale. At least one reference standard was used for every five samples. Corrections were done using a regression method and isotope results are reported in parts per thousand (‰). The analytical uncertainty for δ13C is $\pm$ 0.05‰ (VPDB) and δ18O is $\pm$ 0.14‰ (VPDB), respectively. Of the 117 samples, 2 samples were too small and fell below the device's detection limit (sample vials #305 and #462) (Ankerstjerne, personal communication, 2023).

Chapter 3

Results

3.1 Age-Depth Model

Of the 18 horizons dated by Dr. Serrato Marks, we utilized the 10 ages which fell within the pre-hiatus (older / bottom) section of GC1 in order to generate a constrained age-depth model for this portion. All 10 discrete U/Th ages fell within stratigraphic order (no age reversals) and as such no age was excluded from the model. 2000 Monte-Carlo simulations were run via the COPRA (Constructing Proxy Records from Age models) modeling algorithm, and from these simulations we extracted the median age-depth model and the upper and lower 95% confidence intervals as shown in figure 3.1 (Breitenbach et al. 2012).

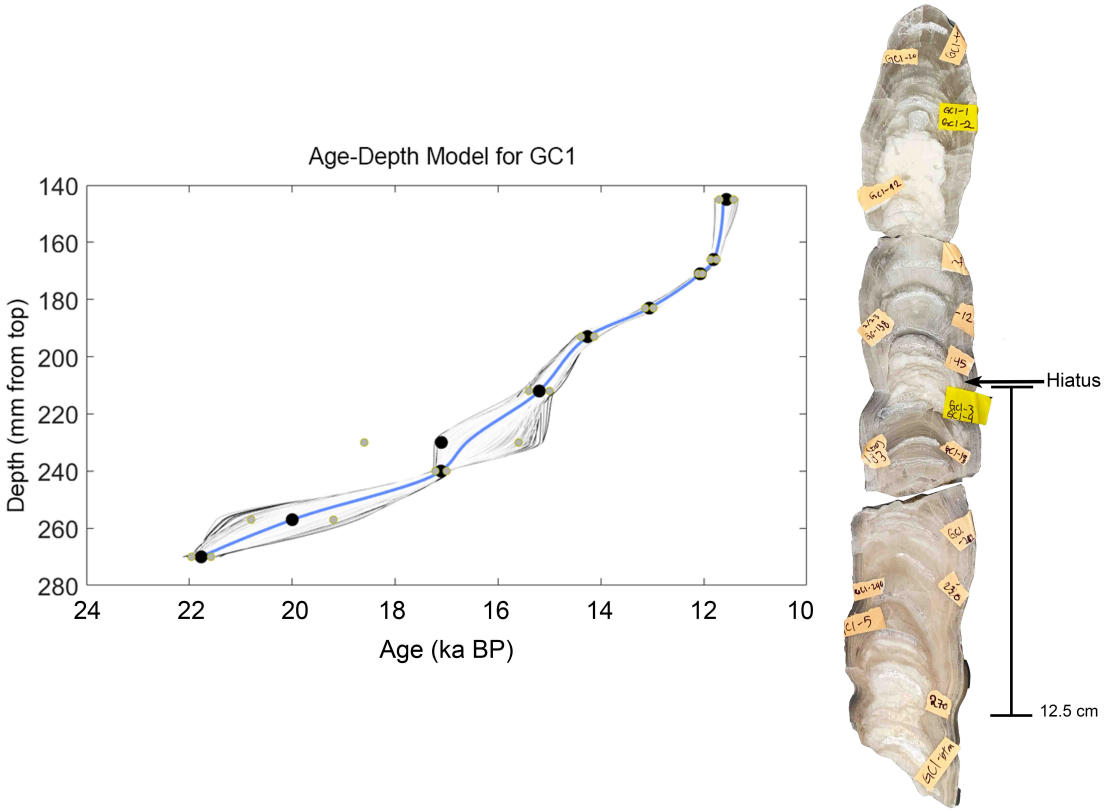

Figure 3-1: Age-depth model for GC1 based on 10 U/Th dates and 2000 Monte Carlo simulations in COPRA (Breitenbach et al. 2012). Median age-depth model is shown in blue; U/Th dates are shown as black dots with associated ±2SD values shown in beige; upper and lower 95% confidence intervals are shown in gray. A photographed cross-section of the stalagmite GC1 is shown to the right (29 cm long). There is a hiatus 145 mm from the top which lasted for approximately 2.7 ka. The older (bottom) section pre-hiatus (145-270 mm from top) is highlighted via the scale bar (12.5 cm long). The full time span of this older (bottom) section is 21.77 ± 1.90 to 11.56 ±1.40 ka BP, where BP indicates years before 1950.

3.2 Stable Isotope and Trace Element Ratios

Here we report proxy data (δ18O, δ13C, Mg/Ca and Sr/Ca) from the bottom portion of stalagmite GC1 (11.56 to 21.77 ka). At an average of 1 mm sampling resolution, the trace element record offers a temporal resolution of 96 years/sample (centennial scale). At just under 1 mm average sampling resolution, the stable isotope record offers a temporal resolution of 82 years/sample (centennial scale).

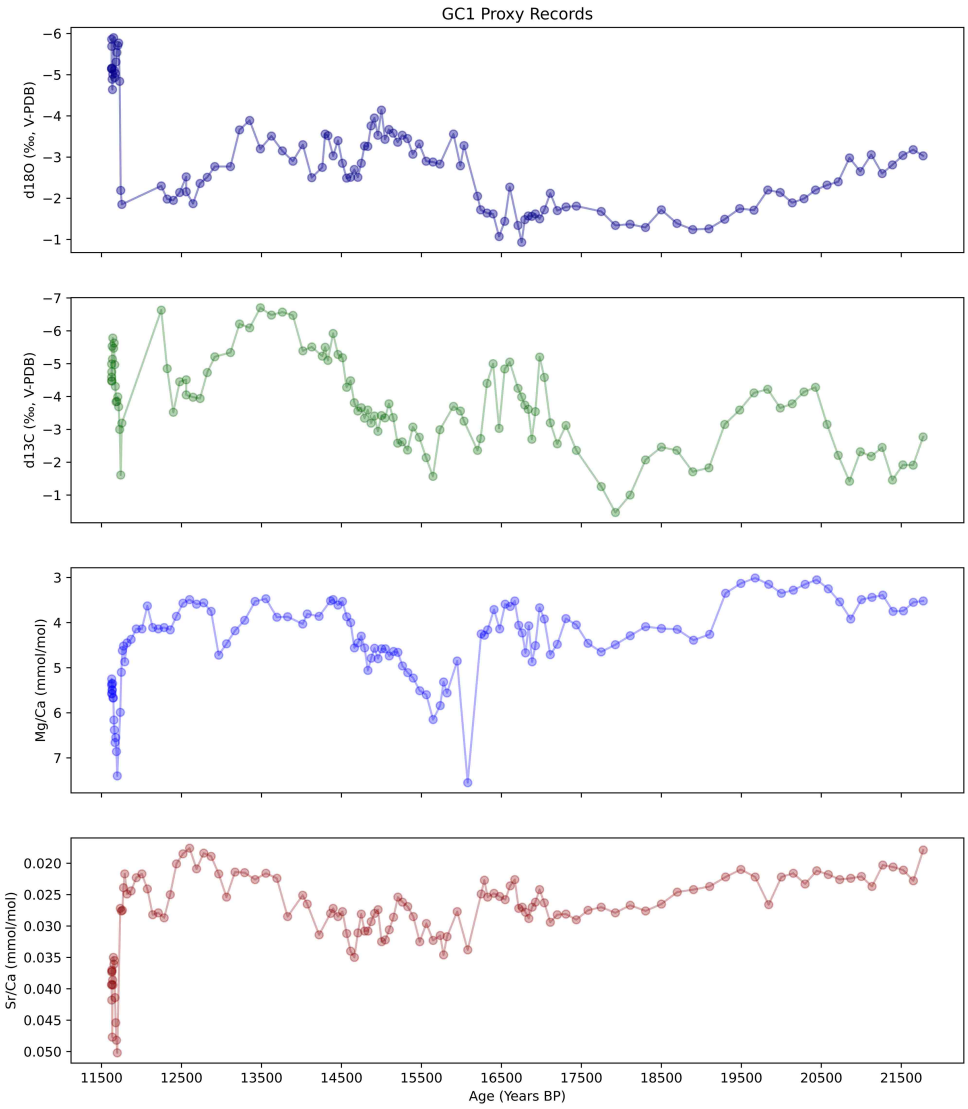

Figure 3-2: Stable isotope (δ18O, δ13C) and trace metal ratios (Mg/Ca, Sr/Ca) for the bottom portion of GC1, plotted along an age profile in years BP, where present is 1950. The record covers the end of the Last Glacial Maximum, Heinrich-Stadial 1, the Bolling-Allerod, and the Younger Dryas Stadial. All records are oriented such that by convention "up" along the y-axis would indicate "wetter" conditions and "down" would indicate "drier" conditions. For further discussion of proxy interpretation, see Section 3.3.

Mean δ18O was -2.90 ± 2.49 ‰ (±2SD), ranging from -0.93 to -5.9. Mean δ13C was -3.80 ± 2.72 ‰, ranging from -6.7 to -0.47. Mean Mg/Ca was 4.43 ± 1.85 mmol/mol, ranging from 1.85 to 7.55, and mean Sr/Ca was 0.03 ± 0.01 mmol/mol, ranging from 0.18 to 0.05. Th/Ca values were not abnormally high, suggesting that the sample has little detrital content).

An abnormally high (low) peak (dip) from the baseline is captured in all four proxy records beginning at approximately 12,000 yBP, towards the end of the Younger Dryas (see Section 4.1). As this spike occurs leading into the hiatus, it is likely that the abrupt jump is not climatic and instead reflects shifting environmental conditions within the cave (e.g. CO2 influx/efflux). The trace element ratios of the younger section of GC1 post-hiatus (8.84 ka BP and younger) immediately return to baseline values of 5 mmol/mol for Mg/Ca and 0.04 mmol/mol for Sr/Ca, further supporting our hypothesis that the spike reflects karst processes rather than a long-term climatic response.

Within the spike leading to the hiatus, two outliers were removed in the Mg/Ca and Sr/Ca records: the first at 11,708 yBP (Mg/Ca = 19.5, Sr/Ca = 0.21), and the second at 11,720 yBP (Mg/Ca = 11, Sr/Ca = 0.07). While there were no signs of instrumental error for these data points, they were not included in Figure 3.2 nor in the calculations above because their abnormally high values obscured variability in the rest of the record.

An additional abnormally high value in the Mg/Ca record at 16,078 yBP (7.55 mmol/mol) was left in the dataset, however, as it fell close to 2SD from the mean and also occurred during Heinrich Stadial 1, during which dry conditions have been well-documented across the northern tropics (See Section 4.1). For example, a compilation of eleven stalagmite records from northern Borneo spanning 0-160 ky BP documents this same extreme dry response with a maximum enrichment in δ18O at 16.3 ka BP (Carolin et al. 2016). Another stalagmite record from the Bahamas spanning 32 to 13.8 ka BP also demonstrates an enriched δ18O spike at 16.2 ka BP (Arienzo et al. 2015). Furthermore, no signs of instrumental error accompanied this spike, and as such the 16.1 ka BP spike of this record was considered a reasonable response.

Finally, while here we report stable isotope values, further discussion of local hydroclimate across the last deglaciation will utilize trace elements (Mg/Ca) as the key indicator of local water balance rather than δ18O (See Section 3.3). This decision is due to the variety of complicated and competing processes in the atmosphere, soil zone, epikarst, and cave system that impact δ18O calcite values, muddying interpretation. A thorough understanding of site-specific cave environmental controls (e.g. infiltration, flow routing, drip seasonality, saturation state, and cave microclimate) can aid interpretation, but even with corroborative data (e.g. δ18O of fluid inclusions, drip water, and local precipitation), δ18O of calcite can reflect multiple controls.

For example: in Israel, calcite δ18O is influenced bys differences between fast-drip and slow-drip waters; in France, the calcite δ18O signal is influenced by the extent of drip CO2 outgassing; and in central Texas, calcite δ18O tracks the changing δ18O values of ocean surface waters of the Gulf of Mexico due to the melting of the Laurentide Ice Sheet (Ayalon et al. 1998; Frisia et al. 2002; Miller et al. 2021). These case studies showcase only a few of the many interpretations of speleothem δ18O and illustrate the pervasive challenge of stable isotope signal interpretation. As of present, no drip water samples have been analyzed from GC1. Consequently, we will further refer to the GC1 δ18O record only to validate the use of the trace element record as a hydroclimate proxy, and not as a rainfall proxy itself.

3.3 Trace Element Interpretation

Modern drip-water studies have demonstrated that marked covariation of Mg/Ca and Sr/Ca ratios in dripwater occurs when a high volume of calcite precipitates upflow of the stalagmite drip, also known as Prior Calcite Precipitation (See Section 1.4) (McMillan et al. 2005; Fairchild et al. 2006). During seasonally "dry" periods, trace element to Ca ratios are enhanced, as upstream PCP preferentially removes Ca relative to Mg and Sr, increasing Mg/Ca and Sr/Ca ratios in drip waters and in downstream stalagmites. Thus, when trace element to Ca ratios co-vary, prior calcite precipitation can be interpreted as an index of aridity (McMillan et al. 2005).

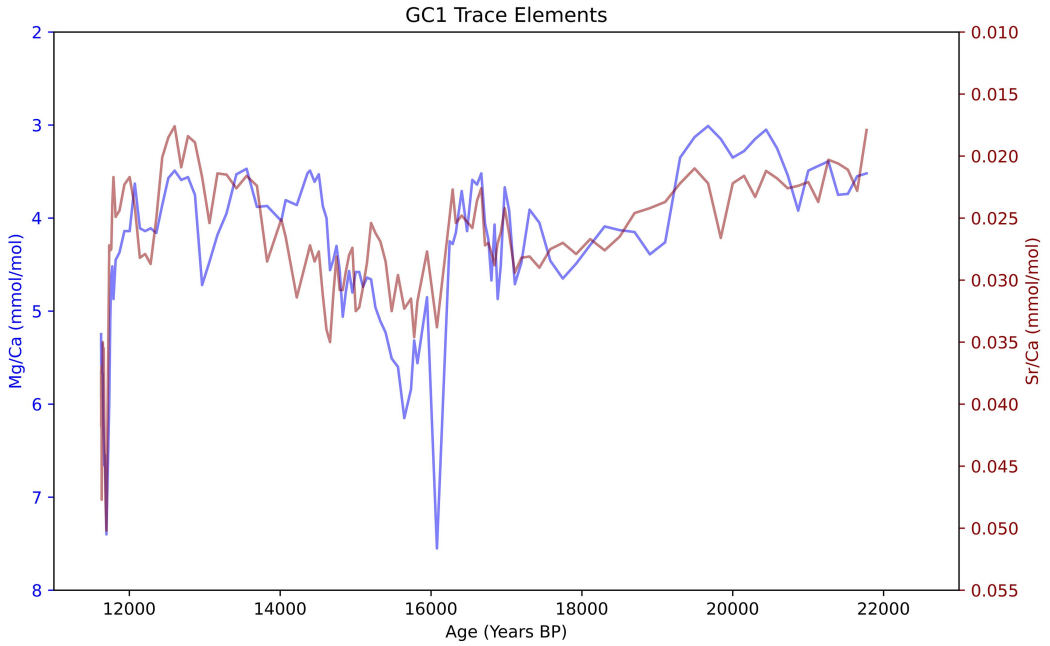

Figure 3-3: Covariation of Mg/Ca and Sr/Ca trace element ratios across the age profile of GC1. While the Mg/Ca dip at 16.1 kya is not captured as strongly in the Sr/Ca record, the majority of the GC1 trace element signal structure exhibits a high degree of synchroneity. This long-term covariation is indicative of a PCP control and implies variations in paleo-aridity (Fairchild et al. 2007).

Several studies have utilized cross-plots to investigate the correlation between proxies and their implications for PCP (Sinclair et al. 2012; Johnson et al. 2006; Frisia et al. 2011). If trace elements reflect the degree of water infiltration to the karst, and if δ13C reflects the rate of degassing, then PCP should drive Mg/Ca, Sr/Ca, and δ13C in similar directions. This relationship is most easily explored by plotting each proxy against the other in turn.

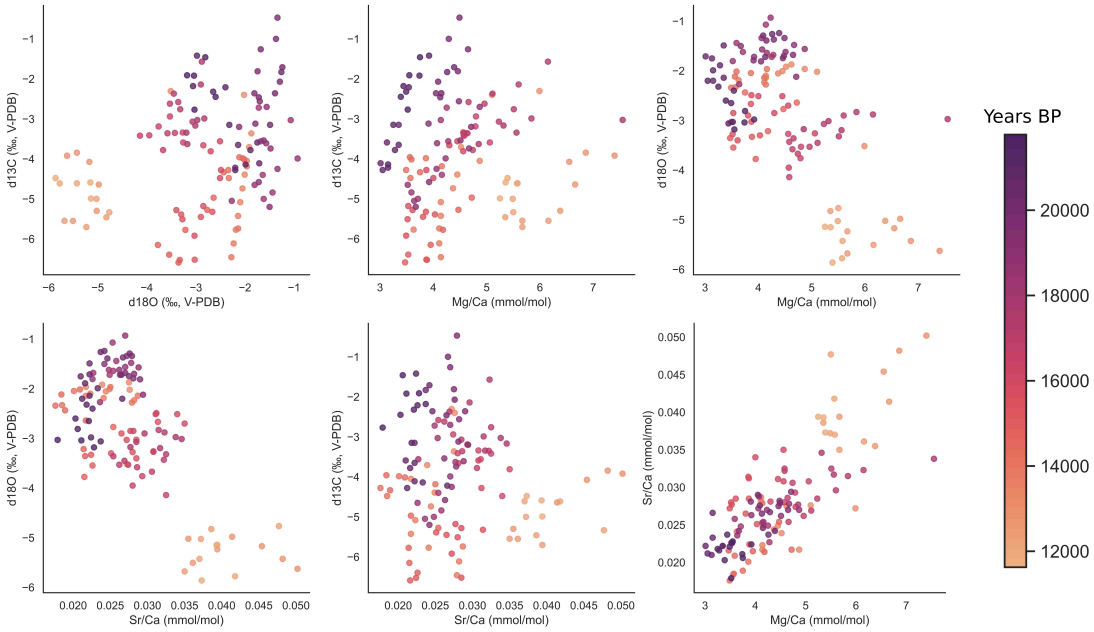

Figure 3-4: Cross-plots of geochemical proxies (δ18O, δ13C, Mg/Ca and Sr/Ca) from GC1 (11.56 $\pm$ 0.14 to 21.77 $\pm$ 0.19 ka). Time series values for stable isotopes were linearly interpolated from the higher resolution trace element dataset to resolve differences in sample resolution and depth-value overlap (Trace elements $\bar{n}$124 vs. Stable isotopes $\bar{n}$115).

Our investigation into all four proxy records yields little covariability between each proxy. δ18O vs. δ13C forms a data cloud with an R2 value of 0.09, indicating no correlation, whereas both δ18O vs. Mg/Ca and δ18O vs. Sr/Ca form data clouds with weakly correlated negative relationships (R2 values of 0.38 and 0.48, respectively). The most promising correlation is that of Mg/Ca vs. Sr/Ca, which exhibits a strong positive relationship (see Fig. 3.5 for further discussion).

While δ13C vs. Mg/Ca does not demonstrate a strongly correlated relationship (R2 = 0.1), when values are plotted by age, a pattern of three disparate positive linear relationships emerges. This same pattern is reflected (albeit more muted) in the δ13C vs. Sr/Ca cross-plot. Because the positive relationships follow three disparate age groups, and because the Mg/Ca vs. Sr/Ca plot is in strong agreement with a PCP control, we interpret the δ13C record as not just a degassing signal but also as a

vegetation signal. A shift in the overlying vegetation (ratio of C3 to C4 plants) would influence the initial δ13C of infiltration waters. This would explain why the cross-plot slope grows less steep over time, but continues to demonstrate PCP when infiltration waters begin with the same isotopic ratio. Based on the observed shift of more negative δ13C values across the deglacial, we expect a shift from C4 to C3 vegetation. We attempt to further investigate this interpretation via fossilized pollen records.

Fossil pollen records are limited in both space and time: to the best of our knowledge, the only nearby record which tracks the Last Deglacial is a sediment core from Lake Chalco in Central Mexico. The record finds a shift from pine-oak forests prior the LGM to open juniper forests and grasslands during the LGM (Lozano-García et al. 2015). As C4 photosynthesis occurs in grasses but not trees, this pollen record substantiates a more dominant C4 signal during the LGM. Furthermore, in the modern day, GC1 is within a pine-oak forest range, which would support a C4 to C3 vegetative shift in the record. Because this is what we observe in the δ13C cross-plot, we confirm that the δ13C is influenced by overlying vegetation, and conclude that its weak correlation can be separated into several strongly correlated PCP-controlled positive relationships.

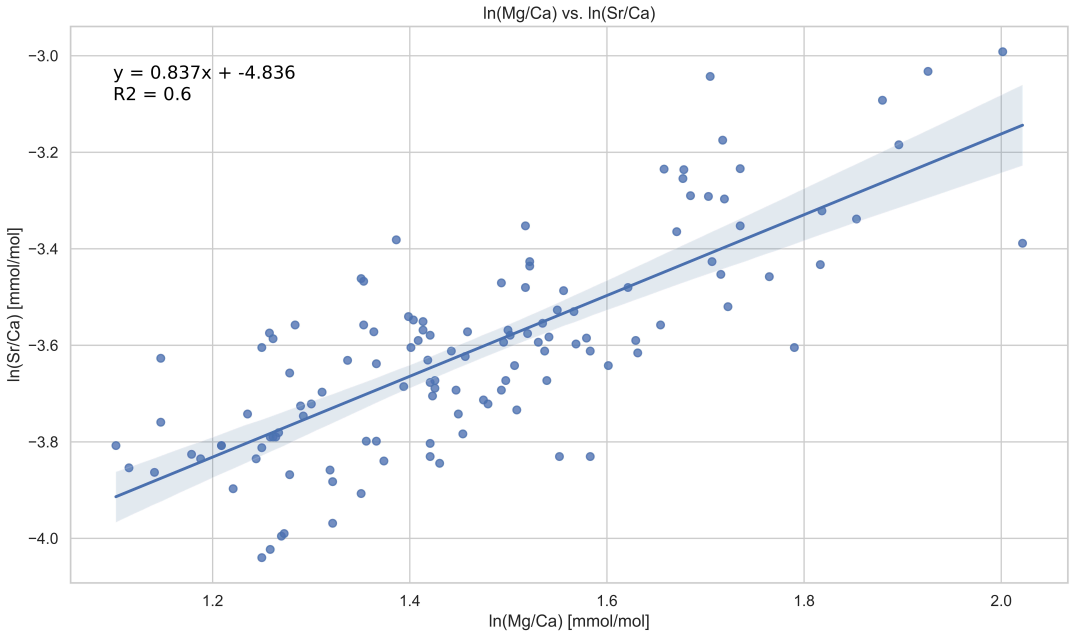

Figure 3-5: Cross-Plot of ln(Mg/Ca) vs. ln(Sr/Ca). The slope is 0.84, which falls within the estimated slope related to prior calcite precipitation (m=0.7-1) (Sinclair et al. 2012). A high correlation coefficient (r2=0.6) indicates that 60% of the variance in Mg/Ca can be explained by the variance in Sr/Ca, suggesting a strong correlation and thus a robust analysis.

The cross-plot of trace element values is consistent with a PCP control. In line with McMillian et al. (2005), this would indicate that PCP reflects the degree of water infiltration into the cave. Therefore, the key question to interpreting the Mg/Ca record is to first define what controls regional water infiltration. In Southern Brazil, high water infiltration ("wet" conditions) in the Mg/Ca record is interpreted as higher levels of precipitation, e.g. rainfall amount (Cruz et al. 2007). In Northeast Mexico, however, modern local water balance is heavily influenced by other factors beyond precipitation, including temperature and relative humidity, which influence the amount of evapotranspiration (Wright et al. 2022).

As a result, we will interpret the change in Mg/Ca ratio to be indicative of local water balance, which is a function of precipitation minus evapotranspiration (P - ET). Any reference to "wet" conditions implies an overall increased local water balance, and

any reference to "dry" conditions implies an overall reduced local water balance. A "wet" period then indicates that the average rate of precipitation is overtaking the average rate of evapotranspiration over the given temporal resolution (96 years/mm), whereas a "dry" period indicates that the average rate of evapotranspiration is overtaking the average rate of precipitation. Depending on neighboring proxies, we will further interpret "wet" or "dry" conditions to be a result of changes in precipitation, changes in evapotranspiration, or both.

3.4 Karst Processes

Lastly, in exploring the impact of karst processes on the trace elements of GC1, stalagmite CB2 offers a useful comparison. Collected along the (wetter) eastern slope of the Sierra Madre Orientales, CB2 is the closest multiproxy speleothem record to GC1, only approximately 900 km Northeast of GC1 and spanning 4.6 to 58.5 ka. Like GC1, the geology surrounding the collection site for CB2 (23.065250° "N, 99.207522° "W, 1071 m.a.s.l.) is composed of Mesozoic limestone-dolomite of the El Abra formation (code KaceCz-Do as assigned by the Government of Mexico Geological Survey). Further geologic information is minimal. As such, the variability in magnitude of Mg/Ca may be a result of the carbonate composition of the karst (limestone vs. dolomite, with dolomite being the less soluble of the two), but without more detailed geologic mapping our interpretation here into karst processes is limited.

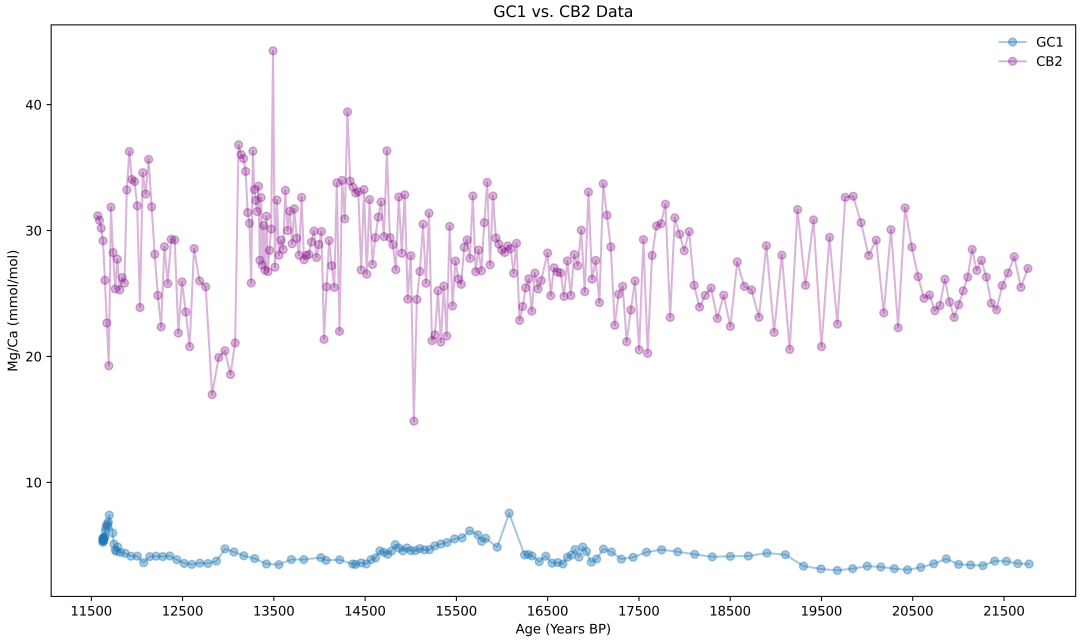

Figure 3-6: Mg/Ca ratios of GC1 and CB2 plotted along an age profile in years BP, where present is 1950. The difference in magnitude between the two stalagmites is likely due to a difference in overlying bedrock geology, with higher trace elements present in the surficial geology at CB2 than at GC1 (Johnson, personal communication, 2023).

It is important to note that absolute Mg/Ca ratios should not be compared across disparate sites for paleoclimate inference for this very reason. Still, future trace element analysis of drip water samples from both sites could pinpoint the extent to which the speleothem calcite trace element composition reflects the composition of the drip waters from which they precipitated, and the amount of PCP in each karst system today. Ultimately, this could assist in a greater understanding of local bedrock-karst interactions and infiltration flowpaths.

Chapter 4

Discussion

4.1 Conditions During Climate Events

Throughout earth's history, there have been a minimum of five major global ice ages: intervals of time (on the scale of tens of millions of years) during which the average planetary temperature decreases and much of the Earth is covered by continental and polar ice sheets. Each ice age is made up of shorter intervals (on the scale of tens of thousands of years) that oscillate between glacial periods (when temperatures drop and glaciers advance) and interglacials (when temperatures rise and glaciers retreat). Glacials and interglacial periods are further divided into stadials (relatively cold periods in the Northern Hemisphere) and interstadials (relatively warm periods in the Northern Hemisphere).

Today, we live in a warm interglacial period during the Quaternary (2.6 mya-present). The most recent period of glacial advance preceding our interglacial today is known as the Last Glacial Maximum; the interglacial period thereafter begins with a transitional period we refer to as the Last Deglaciation. Within the Last Deglaciation, there have been two stadials – Heinrich Stadial 1 (18-14.7 ka) and the Younger Dryas (12.9-11.5 ka) – as well as one interstadial, the Bolling-Allerod (14.7-12.9 ka) (Roy et al. 2016). In this section, we utilize Mg/Ca ratios as a proxy of local water balance (P - ET) as discussed in Section 3.3 to assess how GC1 captures changes in local hydroclimate in response to these four climate events. We also compare

the GC1 record to other regional lake and cave sediment proxies and examine any inconsistencies, so as to ultimately explore drivers of regional climate in Section 4.2.

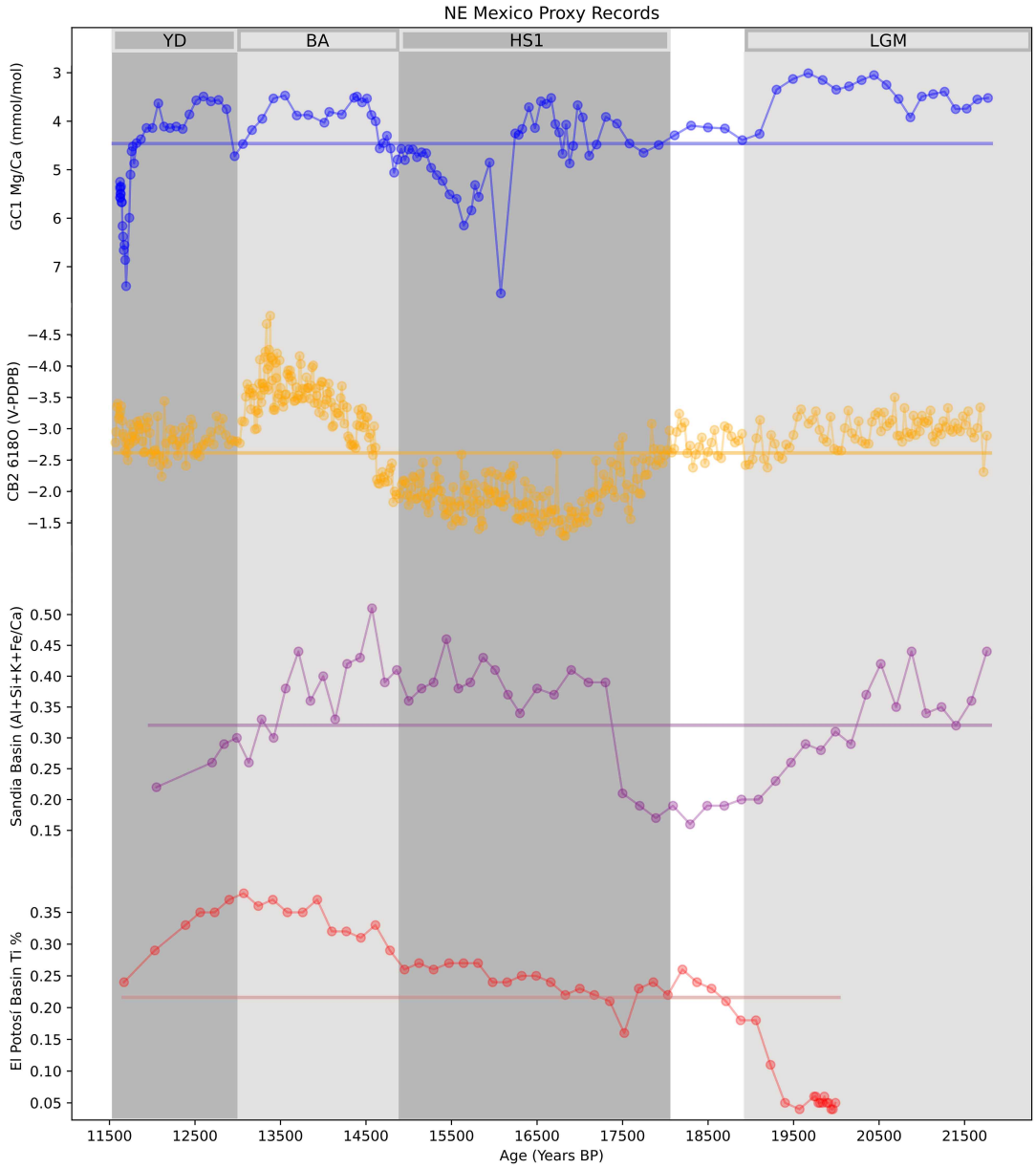

Figure 4-1: A comparison of proxy records across Northeastern Mexico: GC1 speleothem Mg/Ca (blue), CB2 speleothem δ18O (orange; interpreted here as rainfall amount), Sandia Basin lake sediments (purple; abundance of clay minerals interpreted as rainfall amount), and El Potosí Basin lake sediments (red; Ti concentration interpreted as rainfall amount) (this work; Wright et al. 2022; Roy et al. 2020; Roy et al. 2016). For all four records, a "wetter" signal is indicated up along the y-axis and a "drier" signal is indicated down along the y-axis. The mean value for each record is shown via a horizontal line of the same color for ease of reference to background.

Last Glacial Maximum

The Last Glacial Maximum (LGM) peaked at maximum land-based ice volume at approximately 21 ka and terminated at approximately 19 ka with a decrease in ice volume by about 10% (Yokoyama et al. 2000). During the LGM, ice sheets covered much of the Northern Hemisphere. In North America, the Laurentide ice sheet extended as far south as 37ºN to central Missouri, covering most of Northern Canada, the upper American Midwest, Upper Appalachians, and New England with ice as thick as 3 km (Pico et al. 2017; Balco et al. 2010; Gowan et al. 2016).

Northern Mexico hydroclimate responded to the cool glacial conditions of the LGM. A variety of multiproxy datasets, including data from lake sediment cores (e.g. fossil pollen, diatoms, and isotope data), indicate cooler temperatures in the Central American tropics during the LGM (Lachniet et al. 2005). During this period of cooling, reconstructions of sparse vegetation and high dust deposition have argued in favor of a dry climate (Bush et al. 2009). Two of the records presented in Figure 4.1 are also in agreement with a dry LGM. First, the Sandia Basin record (purple) slightly north of GC1 demonstrates a steady decrease in clay mineral percentage, interpreted as decreased erosion rates and thus decreased rainfall. Second, while only covering 21 ka to 19 ka, the El Potosí record (red) further north of Sandia demonstrates decreased Ti % values, also interpreted as decreased erosion rates and decreased rainfall (Roy et al. 2020; Roy et al. 2016).

In stark contrast to these records of dry climate, the two speleothem records presented here instead demonstrate marked "wet" periods. In the GC1 record (blue), we observe an extended period of wet conditions during the LGM (e.g. elevated P - ET) as demonstrated by a 0.99 mean mmol/mol decrease from the baseline mean of 4.43 mmol/mol. In the CB2 record, we also observe an extended wet period, as demonstrated by more negative δ18O values (0.28 ‰ more negative than baseline δ18O). To make sense of this apparent discrepancy between CB2 and expected drying, Wright et al. considers three potential mechanisms: 1) Increased winter precipitation derived from Pacific winter storms, 2) A muted LGM response in NE Mexico due to a weaker Heinrich-Stadial 2 event, or 3) Increased water balance due to colder

temperatures during the LGM, decreasing ET (Wright et al. 2022).

The authors argue against the first mechanism due to CB2 δ18O not reflecting the depleted values expected of a Pacific source. For the second mechanism, they acknowledge a partial contribution to the signal due to foraminiferal evidence of an in complete AMOC shutdown. Ultimately, however, they suggest the third mechanism of decreased temperature as the primary mechanism, as supported by climate models. In particular, Wright et al. references the Paleoclimate Modelling Intercomparison Project (PMIP3) data, which show an increase in the strength of the CLLJ, no increase in winter precipitation, and elevated soil moisture content compared to both the Mid-Holocene and the Pre-Industrial Period (Chevalier et al. 2017).

Furthermore, decreased ET rates are supported by low-altitude, low-latitude groundwater noble gas data, which show widespread six degrees Celsius cooling on land during the LGM (Seltzer et al. 2020). Additionally, work comparing General Circulation Models (GCMs) to pollen and plant fossil databases concludes that during simulations of the LGM, continents generally have wetter topsoils, lower precipitation, and lower photosynthesis (due to low CO2) (Scheff et al. 2017). Other proxy climate records from the Central American tropics which trace evaporation (e.g. lake TIC %, gypsum-clay layers) also capture a wet climate during the LGM corresponding to decreased evaporation (Bush et al. 2009; Lozano-Garcia et al. 2015). Finally, pollen from a lake sediment core in Guatemala indicates vegetation consisting of a temperate pine-oak forest during the LGM, which would require wet topsoils (Hodell et al. 2008).

In conclusion, in line with the work of Wright et al. 2022, the trace element ratio record of GC1 supports a cool-wet climate of Northeast Mexico during the LGM provided that the physical parameter defining wetness is local water balance. This conclusion is supported by the presented body of evidence, which argues in favor of a cool-wet LGM reflecting decreased evapotranspiration rates overtaking decreased precipitation rates in the climate record. Ultimately, like Scheff et al. 2017, this work argues that paleoclimate researchers must take care in defining "wet" and "dry" periods based on the hydrological variable of interest.

Heinrich-Stadial 1

At approximately 18 ka, a massive amount of freshwater was released into the North Atlantic Ocean when a large group of icebergs calved from the Laurentide Ice sheet. This event, known as Heinrich Stadial 1, was one of at least six discharges of icebergs from the North American ice sheets over the last 60 ka. Scientists have worked on reconstructing the timing and extent of Heinrich events via coarse mineral deposits known as ice-rafted debris (IRD) on the floor of the Atlantic Ocean, which were transported by the icebergs as they moved south (Broecker et al. 1992). The causes of Heinrich events remain under debate: one commonly accepted hypothesis states that the cooling conditions of the LGM increased glacial mass, causing instability and calving; another hypothesis suggests that a sudden climate warming event may have accelerated glacial melting, causing sea level rise and disconnecting the glaciers from the ice shelves (Hulbe et al. 2004; Max et al. 2022).

The impacts of Heinrich events on regional climate remain as elusive as their causes. Generally, Heinrich events are considered strongly seasonal: they are associated with extreme winter cooling, but only minor changes in summer temperature (He et al. 2021). Due to the extreme influx of meltwater into the open ocean at southerly locations, Heinrich events are also associated with a slowdown of the AMOC, as the less dense freshwater increases surface buoyancy, suppressing ocean convection (Otto-Bliesner 2010). Of all Heinrich events, Heinrich event 1 in particular has been shown to be the strongest event, with an almost complete AMOC shutdown (McManus et al. 2004).

In Northeastern Mexico, GC1 captures pronounced dry conditions during the middle of Heinrich Stadial 1, with mean values 0.22 mmol/mol higher than baseline. Dry conditions are consistent with the nearby CB2 record, which demonstrates mean δ18O values 0.75 ‰ more positive than baseline δ18O. It is also consistent with proxy records farther south, including a lake sediment core from Lake Chalco in Central Mexico (Lozano-Garcia et al. 2015), a speleothem record from Juxtlahuaca Cave in southwestern Mexico (Lachniet et al. 2015), and the Lake Petén Itzá, Guatemala sediment core (Hodell et al. 2008), all of which show drying through HS1.

In Figure 4.1, two of the proxy records (El Potosi Basin and Sandia Basin) conflict with the expected drying: both demonstrate values elevated from baseline, indicative of a wetter period. However, for both records, this mismatch is likely driven either by uncertainties in the age models and/or the influence of tropical Pacific cyclones during winter precipitation, as lake records are more likely to capture high intensity rainfall events due to their use of erosion as rainfall proxy (Wright et al. 2022). As a result, an increase in extreme climate events may not necessarily track with an overall increase in precipitation. Given these uncertainties, we propose regional drying during HS1 in line with the results of GC1 and the aforementioned proxies.

Furthermore, because Heinrich events only result in minor changes in summer temperature, and because preliminary fluid inclusion microthermometry work has demonstrated only a 1° C increase in tropical warming from the LGM to HS1 (Loland et al. 2022), we suggest that this dry signal is not a result of elevated ET but rather a true precipitation signal. As such, the consistent drying trend across Central America, Southern Mexico, and Northern Mexico can be used to investigate patterns in precipitation across Mexico, such as the north-south precipitation dipole.

The north-south precipitation dipole is a consistent precipitation pattern between northern and southern Mesoamerica, with wet conditions in southern Mesoamerica accompanied by dry conditions in northern Mexico and vice-versa (Wright et al. 2022). This pattern has been simulated across the last two millennia in association with an interbasin gradient of pressure and temperature between the Atlantic and Pacific Ocean, but its continuity on longer timescales is still an area of active research (Bhattacharya et al. 2017).

In assessing the response of the proxy records presented in this section, we note that rather than a precipitation dipole between the northern and the southern records, we observe spatially uniform drying. This may be because the strength of HS1 is extreme enough to trigger nearly 10° C of cooling across the Atlantic Basin, as calculated via an isotope-enabled Earth System Model Simulation (Wright et al. 2022). The freshwater forcing model demonstrates that with extreme cooling across the Atlantic Basin, the Atlantic-Pacific pressure gradient strengthens, increasing the strength of

CLLJ. Unlike modern seasonal strengthening of the CLLJ, the model results show that combined strong winds and strong SST cooling results in decreased moisture flux across Mesoamerica, in accordance with our presented proxies (Wright et al. 2022). The role of these climate forcings in the GC1 record will be further explored in Section 4.2.

Ultimately, this work supports a cool-dry response in Northeastern Mexico during Heinrich Stadial 1, while suggesting that for extreme climate events such as strong Heinrich stadials, the dipole precipitation response does not dominate on orbital to millennial timescales.

Bolling-Allerod Warming

Immediately following the cool-dry climate of Heinrich Stadial 1, the Bolling-Allerod (B/A) interstadial was a period of abrupt warming which lasted from 14.7 to 12.9 ka ka. Recent studies have linked the abrupt warming period to a strengthening of the AMOC caused by the release of warm waters from the deep North Atlantic Ocean, which built up over the course of Heinrich Stadial 1, as well as increased greenhouse gas concentrations (Su et al. 2016).

During the B/A, GC1 captures an increased and sustained "wet" period, with mean values 0.52 mmol/mol lower than baseline. This signal is supported by all three of the nearby proxy records. The elevated Potosí Basin Ti % signal (0.13% more positive than baseline) and the more negative CB2 δ18O signal (0.73‰ more negative than baseline) both indicate increased and sustained precipitation during this time (Roy et al 2016; Wright et al. 2022). The clay minerals of the Sandia Basin also capture a wet signal, with mean values 0.04% more positive than baseline, but these values decrease across the B/A, possibly as a result of uncertainties in the lake sediment age model. The wet signal is captured in Central Mexico as well, as the Lake Chalco core finds higher amounts of runoff during the B/A corresponding to more frequent high-intensity storms (Roy et al. 2020). Farther south, the Petén Itzá core also demonstrates moist conditions from 14.7 to 12.8 ka, with a brief return to dry conditions at 13.8 ka that is mirrored in the GC1 record by a drier period lasting

from approximately 14.2 to 13.8 ka. This dry dip coincides with the Older Dryas and meltwater pulse 1A, a period of rapid sea-level rise in the Caribbean Sea as a result of further collapse of the North American ice sheet (Hodell et al. 2008).

All three of the sustained "wet" records (GC1, CB2, and the Potosí Basin) demonstrate a slight lag in response to the B/A, with a shift from initial dry conditions to wet conditions not corresponding perfectly to the onset of the B/A. This time lag is likely due to changing vegetation as a result of the abrupt rise in atmospheric CO2 at the onset of the B/A, or due to the time required to refill the groundwater aquifers following the extreme dry period of Heinrich Stadial 1 (Kohler et al. 2011).

In general, there is strong regional coherence of wetter conditions across Mesoamerica during the Bolling/Allerod. In Northeast Mexico, lake sediment records and speleothem records demonstrate both an increase in the frequency of high intensity precipitation events as well as average precipitation.

Younger Dryas

The Younger Dryas (YD) was a period of abrupt cooling from 12.9 to 11.5 ka. The prevailing hypothesis for the cause of the YD is that as the planet warmed through the deglacial period due to orbital forcing, glacial flood waters from the melting Laurentide Ice Sheet emptied into the Arctic and the North Atlantic. This massive influx of freshwater diluted Atlantic salinity, thus decreasing the density of surface water so that it could no longer sink, leading to a shutdown of the AMOC (Partin et al. 2015). Like during HS1, Atlantic SSTs of the Younger Dryas experienced marked cooling (more than 5°C) as simulated by climate models (Renssen et al. 2018). At the same time, greenhouse gasses (including CH4) increased (Raynaud et al. 2000).

Due to the decrease in Atlantic SSTs, we expect to see a dry response during the Younger Dryas. Though CB2 seems to capture a signal closer to the muted LGM wet signal, an ice volume correction shifts the YD record closer to the dry conditions of HS1 (Wright et al. 2022). The Sandia Basin record captures a decrease in storm events via mean values 0.07 lower than baseline, and though the Potosi Basin Ti % record is still elevated from baseline, it decreases throughout the YD, interpreted as a

gradual reduction in precipitation (Roy et al. 2020). In the Petén Itzá core, the onset of the Younger Dryas at 12.8 marked the return of gypsum and thus dry conditions (Hodell et al. 2008).

In contrast to these dry conditions, the GC1 record captures wet conditions up until the mid-to-late Younger Dryas, during which there is an abrupt drying spike leading up to the hiatus. This is likely due to karst processes which contributed to the pause in growth at the hiatus. While there is no sign of instrumental error or detritus for these values, the cause of the wet YD in the GC1 record remains unclear. Regional discrepancies during the Younger Dryas are not uncommon: in the Western tropical Pacific, the hydroclimate responses to the YD are also spatially and seasonally variable (Partin et al. 2015). However, up until this period, the hydroclimate variability recorded in GC1 demonstrated strong coherence with the CB2 speleothem record. As such, results from an additional speleothem record would be helpful to further investigate this abrupt period of incoherence, especially as the end of Younger Dryas may be a useful analogue to the impact of future anthropogenic global warming on tropical precipitation (See Section 5).

4.2 Climate Forcings

Multiple dynamic and thermodynamic climate forcings have been considered as drivers of precipitation over Northeast Mexico on millennial to orbital scales. Paleoclimate studies have explored increased SSTs in the North Atlantic, AMOC strengthening, ITCZ southward displacement, increased insolation, high Atlantic-Pacific SST gradients, and atmospheric pCO2 in connection to increased precipitation (see Section 1.3 for more). Of these many drivers, recent studies have emphasized the role of Atlantic SSTs in modulating NE Mexico hydroclimate, with higher Atlantic SSTs leading to increased precipitation as well as more frequent high-intensity rainfall events, even during periods of less total annual precipitation (Wright et al. 2022; Roy et al. 2020). However, one limitation to these correlations is the paucity of high-quality SST records from the Atlantic. Promising new climate simulation results from Bhattacharya et

al. (2020) show that during the Common Era, a low Atlantic-Pacific SST gradient (high Atlantic-Pacific SLP gradient) is associated with a strengthening of the CCLJ and a southward displacement of the ITCZ, resulting in a drier NE Mexico. Because these results are confined to the last two millennia, here we choose to investigate the correlation between the Atlantic-Pacific SST gradient and the GC1 record on a longer millennial to orbital timescale spanning 21.77 ka to 11.56 ka.

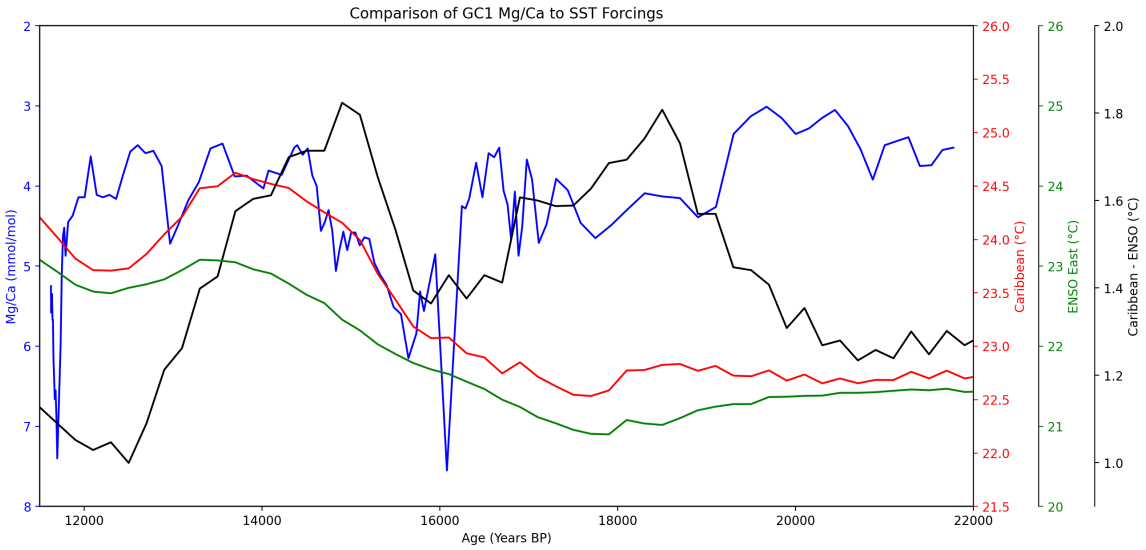

Figure 4-2: The GC1 Mg/Ca record (blue) plotted against Caribbean SSTs (red), ENSO East SSTs (green), and the Caribbean-ENSO SST gradient (black) from 22,000 yBP to 11,500 yBP. SSTs were sourced from the Last Glacial Maximum Reanalysis model (Osman et al. 2021). Note that the SST y-axes are not equal: Caribbean y-min is set at 21.5 °C to emphasize visual gradient between SSTs.

To investigate SST correlation, SSTs were calculated using the Last Glacial Maximum Reanalysis (LGMr) from Osman et al. (2021), a model which leverages climate simulations and proxy data to trace surface temperature change spanning the Last Glacial Maximum to present at 200-year resolution. Atlantic SSTs were calculated from the Caribbean Sea at a latitudinal slice of 9 to 22 decimal degrees and a longitudinal slice of 271 to 300 decimal degrees (as determined via Lea et al. 2003). Pacific SSTs were calculated in the tropical Pacific, slightly north of ENSO regions 1 and 2 due to their proximity to the western coast of Mexico, at a latitudinal slice of -5 to 5 decimal degrees and a longitudinal slice of 268 to 279 decimal degrees.

Visible correlation between the GC1 Mg/Ca record and the Atlantic-Pacific SST gradient supports the work of Bhattacharya et al. and Wright et al. During the LGM, the inverse correlation between GC1 and Atlantic-Pacific SSTs is due to the GC1 wet signal not tracking precipitation. Between 19 and 15 ka, the two records show moderate to strong covariance, with the lag between the forcing and the record not uncommon in paleoclimate studies (Yang et al. 2022). Most promising, the strong drying period during Heinrich Stadial 1 corresponds to a significant weakening of the Atlantic-Pacific SST gradient, as expected from Section 4.2. During this time period, the weak SST gradient leads to an anomalously high Atlantic-Pacific SLP gradient, strengthening the easterlies to such a degree that the rain whips past NE Mexico without raining out. During the Bolling-Allerod, Atlantic SSTs increase significantly, as expected from the release of deep ocean heat, while Pacific SSTs increase at a lower rate, enhancing the SST gradient and corresponding to a wet NE Mexico. The two SST records begin to decrease during the Younger Dryas while the gradient simultaneously decreases, but the GC1 record does not perform as expected during this period, and as such this period requires further investigation with other climate forcings.

In conclusion, as the Wright et al. (2022) record differs in hydroclimate response from the regional lake records, the GC1 record is especially constructive in confirming the results of this foundational work. Furthermore, the interpretations of Wright et al. are expanded upon in this work via the preliminary demonstrated coherency between GC1 Mg/Ca and the Atlantic-Pacific SST gradient rather than Atlantic SST variations alone. The work of Bhattacharya et al., too, is further supported on a proxy timescale more than ten times that of the original simulation. Ultimately, on millennial to orbital timescales, moisture transport in NE Mexico across the last deglacial is closely linked to variability in the Atlantic-Pacific SST gradient.

4.3 Climatic Background for First Peopling

In Section 1.2, we introduce the hypotheses of the First Peopling of the Americas as two disparate camps: the "Kelp Highway" route and the "Ice Free Corridor" route. However, these two camps are in fact not mutually exclusive, and a combination of the two is highly probable (Potter et al. 2018). First peoples may have traveled both along the coasts as well as inland, either in multiple stages of one genetic group or as different genetic groups. Even along the "Kelp Highway" route, first peoples may have continued eastward and/or southward via an inland route after making contact with the Pacific Coast of North America.

In exploring the concurrence of both options, genetic evidence suggests that several distinct population branches emerged from a single population group of East Asian-North Siberians, who were genetically isolated from 25 to 18 ka BP (Raff et al. 2014). At 18 ka BP, the single group split into three groups: one returned to Siberia, another became isolated in Alaska, and the third spread rapidly south of the ice sheets as early as 17 ka BP. The authors argue that this rapid dispersal was more likely to occur by boat than by an inland route, including through the use of boating into the interior of the North American continent along riverways.

Despite the emerging body of evidence in favor of the "Kelp Highway," inland movement is still likely to have occurred, as all of the earliest American sites are entirely terrestrial. While key Pleistocene coastal sites along the Pacific would have been submerged by rising seas following the last glacial maximum (Braje et al. 2017), we would still expect to see more recent surviving sites (Potter et al. 2018). This reflects a larger limitation in occupation timing interpretation: the existence of sites from a certain time period only reflects that those site remains survived to the present day, not that those sites represent the earliest settling of the region, as there may always be new finds to push dates farther back. Furthermore, each younger site may not represent the entire upheaval and relocation of one older site; it is possible that older sites split prior to movement, with partial communities remaining in place.

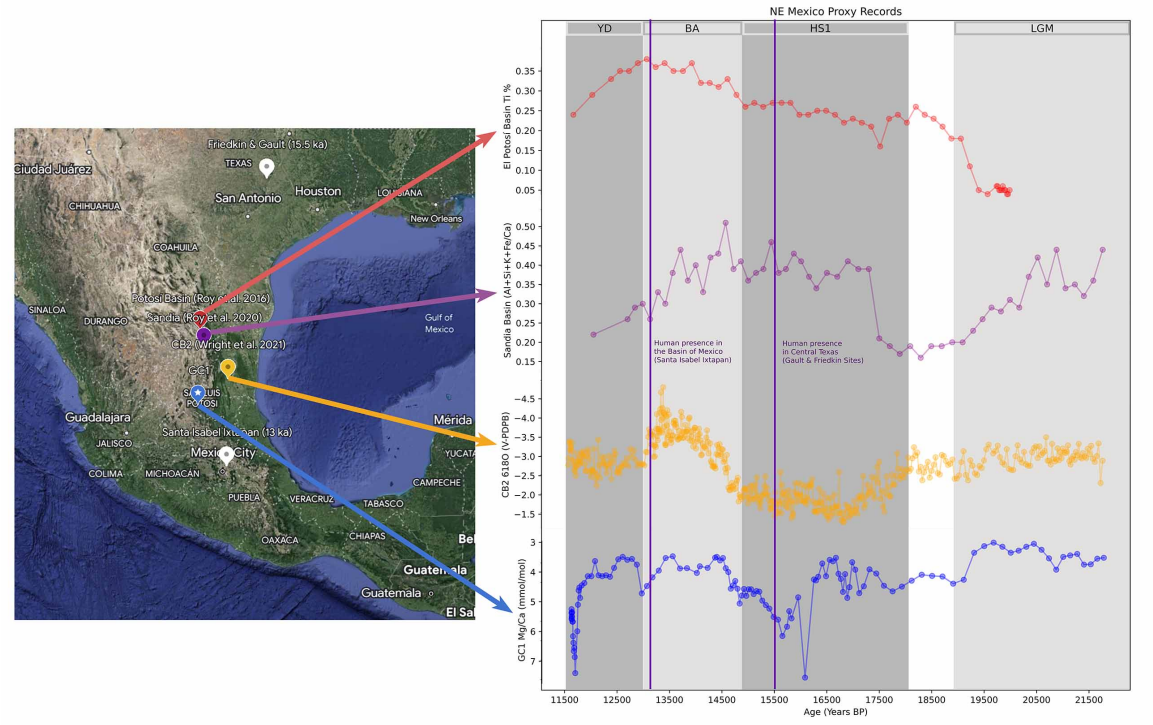

Figure 4-3: Select proxy records from north to south: El Potosí Basin lake sediments (red; Ti concentration interpreted as rainfall amount), Sandia Basin lake sediments (purple; abundance of clay minerals interpreted as rainfall amount), CB2 speleothem δ18O (orange), and GC1 speleothem Mg/Ca (blue) (Roy et al. 2016; Roy et al. 2020; Wright et al. 2022). For all four records, a "wetter" signal is indicated up along the y-axis and a "drier" signal is indicated down along the y-axis. The map inset (left) includes two archaeological sites in white pins from north to south, which are indicated as purple lines in the proxy record (right) from right to left: the Friedkin & Gault site (15.5 ka) and the Santa Isabel Ixtapan Site (13 ka) (Williams et al. 2018; Ochoa et al. 2021). The climate of Northeastern Mexico between the earliest occupation of the two sites is marked by the warm Bolling-Allerod interstadial, which appears wet in all three proxy records save from the Sandia Basin.

Regardless of these discrepancies and limitations, the hydroclimate reconstruction of Northeastern Mexico as presented in this thesis can provide insight into periods of regional drought and periods of regional water availability which impacted early human movement and environmental adaptation. In the case that early peoples were traveling inland by boat, periods of drought would have impacted available riverways, especially as droughts in the region are known to last decades to centuries (Bhattacharya et al. 2020). For groups traveling by foot, freshwater bodies would have been equally important for settling: movement into the interior of the continent likely prioritized riverbank and lakeshore ecosystems (Dillehay 2000). Thus the GC1 proxy record can help indicate periods in which these freshwater resources would have been abundant or under stress.

The two archaeological sites explored in this thesis are the Friedkin & Gault site of central Texas, north of the GC1 study site, and the Santa Isabel Ixtapan site in Central Mexico, south of the GC1 study site (Williams et al. 2018; Gonzalez et al. 2003). The sites were chosen due to their uncontested dating results, their geographic proximity to the GC1 study site, and their potential capture of chronological southward movement (from the older northern site to the younger southern site). At the Friedkin & Gault site, optically stimulated luminescence age estimates found dates from 15.5 to 20 ka in association with early projectile point technology unrelated to Clovis-era stone tools or any other typological group found in the Basin of Mexico. As a conservative approach, we mark Friedkin & Gault at 15.5 ka in Figure 4.3. At the Santa Isabel Ixtapan site located on the margins of Lake Texcoco, seven mammoth skeletons were found with stone flakes embedded in the bones, some with deep cut marks, suggesting a mammoth kill site. Like at Friedkin & Gault, the flint projectile points were not of Clovis typology, but unlike Friedkin & Gault, they were assigned a regional classification (Lerma typology). Tephra dating of ash pockets within the same stratigraphic layer found oldest dates between 14.5 and 13 ka (again we mark the younger bound of the two).

If we are to assume a general southward movement from the older, upper site to the younger, lower site, the GC1 record can provide insight into the climate early

peoples may have encountered along the journey. As discussed in Section 4.1, between 15.5 and 13 ka, GC1 captures an increased and sustained "wet" period out of Heinrich Stadial 1 and through the Bolling-Allerod warming. This signal is supported by two of the three nearby proxy records (with the third dry signal possibly a result of uncertainties in the age model). As such, early humans migrating southward would have done so during a wetter period than their more recent past. This observation is in contrast with the generally accepted model of early human migration, in which communities moved in response to water stress: it was an ancient drought that drove early human migrants out of Africa and into the Levant 65 ka, and in Pleistocene - Holocene environments across the globe, ancient droughts have corresponded to regional expansion and population movement to resource-rich areas (Groucutt et al. 2015; Petragalia et al. 2020; Sear et al. 2020).

To make sense of this apparent discrepancy, here I will introduce three preliminary interpretations in order of this author's consideration of plausibility. First, if we accept the model that early human migration is most often driven by water stress, and given that the projectile point typology of the two sites is not a clear match, it is possible that these two sites are not related and are instead inland sites of separate waves of eastward movement. This interpretation would support the Kelp Highway hypothesis, as it assumes a Pacific Coast landing and subsequent movement therefrom. This interpretation is substantially strengthened by a record from the Santiaguillo ephemeral lake, located west of of the sites and the proxy records presented in thesis, which captures a peak of extreme drought conditions lasting from 20 to 13 ka as demonstrated by below-average detrital minerals and (Ti/Ca) and above-average calcite precipitation (the most elevated values in the last 90 ka) (Quirox-Jiménez et al. 2017). This period of drought would have likely driven the communities from the coast eastward in search of resources, where once they encountered the wet conditions of Northeastern Mexico during the Bolling-Allerod, they settled long enough for sites to be preserved.

The second interpretation recognizes that between the two sites, nearly 2.5 ka of time passes, and within millennial-scale periods of increased precipitation, there

can still be shorter periods of localized drought on the decadal or centennial scale (Bhattacharya et al. 2020). Because these records do not offer quantitative inferences into the degree of drying or increased rainfall, it can be difficult to deduce the extent to which these smaller variations in the record impacted early human movement. Still, as the record presented in this work is on a centennial scale, we can suggest that more positive Mg/Ca values (e.g. 14.5-13.5 ka) represent a drier period within the context of the wetter Bolling-Allerod that may have generated southward movement.

The third interpretation assumes a connection between the two archaeological sites in-line with the Ice Free Corridor southward movement, but requires a novel approach to the motivation behind early human movement. If communities moved southward during periods of water availability, it would have been "pull" factors of increased water availability and freshwater resources and not "push" factors of increasing drought that drove them to do so. In this interpretation, early communities would have utilized the abundant lakes as a means to support their journey, such as in the case of the peopling of the Saharas during Green Sahara periods (D'Atanasio et al. 2018). This interpretation would require rethinking the common motivation behind why people move – if this record does not capture a story of those in search of better conditions, perhaps it is a record of early human curiosity and ambition.

Ultimately, offering a definitive insight into the First Peopling of the Americas is beyond the scope of this thesis. Nonetheless, the concurrence of a dry western shore with a wet eastern shore offers a promising insight into regional movement. Additionally, noting coherency between three of the four Northeastern Mexico paleoclimate records during a crucial time in the history of the first peopling is valuable as a baseline for future study. Increasing the spatial resolution of paleoclimate records along the Pacific coast of Mexico would be especially useful in providing a background to the Kelp Highway hypothesis.

Chapter 5

Conclusion

Highlights

- A speleothem from San Luis Potosí, Mexico spanning 21.77 to 11.56 ka BP was used to reconstruct hydroclimate in Northeast Mexico at centennial resolution
- Trace element ratios exhibited a Prior Calcite Precipitation control and were determined to reflect local water infiltration (P - ET)
- The record indicates a wet response during the LGM, a dry response during Heinrich-Stadial 1, and a wet response during the Bolling-Allerod
- On millennial to orbital timescales, moisture transport in NE Mexico across the Last Deglaciation is linked to the Atlantic-Pacific SST gradient
- Regional climate insights support the Kelp Highway hypothesis
- Our results substantiate the results of speleothem CB2 from the Last Glacial Maximum through the Bolling-Allerod (Wright et al. 2022), indicating consistent climate responses across orographic barriers on millennial timescales

Conclusions and Future Work

This thesis presents a new, high-resolution stalagmite record from Northeastern Mexico spanning 21.77 to 11.56 ka BP. Using the Mg/Ca record as a proxy for past hydrological change (P - ET) in the region, we observe a wet response during the Last Glacial Maximum, a dry response during Heinrich Stadial 1, a wet response during the Bolling-Allerod Warming, and variable conditions during the Younger Dryas. We compare our record to nearby proxies in Northeastern Mexico and Southern Mesoamerica as well as climate models to investigate regional coherency and climate forcings on millennial to orbital timescales.

Our hydroclimate observations have implications for defining glacial climate and assessing the North-South precipitation dipole on millennial timescales. In response to the presumed discordance between regional proxies and in line with recent climate models, we define the LGM as a period of both decreased precipitation and decreased evaporation. Additionally, our work demonstrates spatially homogeneous drying during Heinrich Stadial 1 and spatially homogeneous wet conditions during the Bolling-Allerod warming. As a result, we suggest that the modern-day Mesoamerican North-South precipitation dipole does not dominate on orbital to millennial timescales. Furthermore, during Heinrich Stadial 1 and the Bolling-Allerod, we find good coherency between moisture transport in NE Mexico and the Atlantic-Pacific SST gradient. Finally, our investigation into paleolithic archaeological sites and our comparison of the climates of Eastern and Western Mexico during the Bolling-Allerod yields strong support for the Kelp Highway hypothesis.

While the data presented in this thesis provides new insights into the climate of Northeastern Mexico across the Last Deglaciation, there are still myriad opportunities for future investigation. First, we aim to continue the preliminary exploration of climate forcings as presented in Section 4.2. Observed discrepancies between the Atlantic-Pacific SST gradient and the terminus of the Bolling-Allerod / onset of the Younger Dryas may be explained by separate or additional controls, especially the rise of greenhouse gasses. Second, increasing the spatial resolution of paleoclimate records along the Pacific coast of Mexico would improve our understanding of the

spatial extent of localized drought during this time period and its implications for early human migration patterns.

Third, past periods of climate variability can serve as analogues for future global warming. As anthropogenic global warming increases, multiple climate models predict a moderate to near-complete AMOC shutdown as a result of the Northern Hemisphere warming at a faster rate than the Southern Hemisphere as well as increased greenhouse gas forcing (Shakun et al. 2012; Liu et al. 2017; Boers 2021). Of the recent geologic past, the Younger Dryas cooling can serve as an analogue to a period of increased greenhouse gas forcings and a weakening AMOC. Investigating the regional hydroclimate responses of this time period can inform our predictions of the impacts of greenhouse gasses and AMOC weakening on water availability in Northeastern Mexico and the tropics. For this reason, increasing the spatial resolution of paleoclimate records from the tropics spanning the full Younger Dryas is a compelling avenue for future work.

Finally, while in this work we introduce a stable isotope record at approximately centennial resolution, we do not present this record as a direct paleoclimate and/or paleoenvironment proxy. Future iterations of this work would benefit from a comparison of δ18O of calcite to δ18O of cave drip water and local precipitation so as to utilize stable isotope data to interrogate trace element insights.

Appendix A

Appendix A. Data

Table A.1: Stable isotope and trace element data for stalagmite GC1 pre-hiatus. Age is given as year before present (1950 CE). Data are organized by increasing depth (measured from the top of the stalagmite) and span multiple pages. Missing data are noted with NaN.

Depth (mm from top)	Age (Years BP)	Mg/Ca (mmol/mol)	Sr/Ca (mmol/mol)	d18O (‰, V-PDB)	d13C (‰, V-PDB)
144.5	11625	5.2488	0.0394	-5.14	-4.99
145.5	11625	5.3550	0.0393	-5.15	-4.59
146.5	11626	5.3914	0.0373	-5.86	-4.48
147.0	11626	5.5700	0.0418	NaN	NaN
147.5	11627	NaN	NaN	-5.69	-4.75
148.0	11628	5.5800	0.0370	NaN	NaN
148.5	11629	NaN	NaN	-5.16	-4.47
149.0	11630	5.4900	0.0372	NaN	NaN
149.5	11631	NaN	NaN	-4.89	-5.53
150.0	11633	5.5000	0.0477	NaN	NaN
150.5	11635	NaN	NaN	-4.64	-5.14
151.0	11637	5.3500	0.0386	NaN	NaN
151.5	11639	NaN	NaN	-5.01	-5.78
152.0	11641	5.6700	0.0394	NaN	NaN

Depth (mm from top)	Age (Years BP)	Mg/Ca (mmol/mol)	Sr/Ca (mmol/mol)	d18O (‰, V-PDB)	d13C (‰, V-PDB)
153.0	11647	5.6700	0.0350	NaN	NaN
153.5	11650	NaN	NaN	-5.9	-5.47
154.0	11653	6.1600	0.0361	NaN	NaN
154.5	11656	NaN	NaN	-5.11	-5.63
155.0	11660	6.3800	0.0355	NaN	NaN
155.5	11664	NaN	NaN	-4.93	-4.97
156.0	11668	6.6600	0.0414	NaN	NaN
156.5	11672	NaN	NaN	-5.03	-4.31
157.0	11677	6.5500	0.0454	NaN	NaN
157.5	11682	NaN	NaN	-5.31	-3.84
158.0	11687	6.8600	0.0482	NaN	NaN
158.5	11692	NaN	NaN	-5.54	-3.85
159.0	11697	7.4000	0.0502	NaN	NaN
159.5	11703	NaN	NaN	-5.71	-3.99
160.5	11715	NaN	NaN	-5.77	-3.69
161.5	11726	NaN	NaN	-4.84	-3
162.0	11733	5.9900	0.0272	NaN	NaN
162.5	11740	NaN	NaN	-2.19	-1.61
163.0	11747	5.1000	0.0276	NaN	NaN
163.5	11754	NaN	NaN	-1.85	-3.19
164.0	11761	4.6200	0.0275	NaN	NaN
165.0	11775	4.5200	0.0239	NaN	NaN
166.0	11791	4.8700	0.0217	NaN	NaN
167.0	11819	4.4500	0.0249	NaN	NaN
168.0	11870	4.3700	0.0244	NaN	NaN
169.0	11935	4.1400	0.0223	NaN	NaN
170.0	12005	4.1400	0.0217	NaN	NaN
171.0	12073	3.6300	0.0241	NaN	NaN
172.0	12140	4.1100	0.0282	NaN	NaN

Depth (mm from top)	Age (Years BP)	Mg/Ca (mmol/mol)	Sr/Ca (mmol/mol)	d18O (‰, V-PDB)	d13C (‰, V-PDB)
173.0	12210	4.1400	0.0279	NaN	NaN
173.5	12246	NaN	NaN	-2.3	-6.63
174.0	12282	4.1100	0.0287	NaN	NaN
174.5	12320	NaN	NaN	-1.98	-4.85
175.0	12358	4.1600	0.0250	NaN	NaN
175.5	12397	NaN	NaN	-1.95	-3.52
176.0	12437	3.8600	0.0201	NaN	NaN
176.5	12477	NaN	NaN	-2.14	-4.45
177.0	12517	3.5700	0.0185	NaN	NaN
177.5	12559	NaN	NaN	-2.52	-4.51
178.0	12601	3.4900	0.0176	NaN	NaN
178.5	12644	NaN	NaN	-2.16	-4.05
179.0	12687	3.5900	0.0209	NaN	NaN
179.5	12732	NaN	NaN	-1.87	-3.98
180.0	12777	3.5600	0.0184	NaN	NaN
180.5	12822	NaN	NaN	-2.36	-3.94
181.0	12868	3.7500	0.0189	NaN	NaN
181.5	12915	NaN	NaN	-2.51	-4.73
182.0	12963	4.7200	0.0217	NaN	NaN
182.5	13011	NaN	NaN	-2.77	-5.21
183.0	13060	4.4700	0.0254	NaN	NaN
183.5	13111	NaN	NaN	-2.77	-5.34
184.0	13167	4.1800	0.0214	NaN	NaN
184.5	13225	NaN	NaN	-3.66	-6.21
185.0	13288	3.9500	0.0215	NaN	NaN
185.5	13351	NaN	NaN	-3.89	-6.09
186.0	13417	3.5300	0.0226	NaN	NaN
186.5	13484	NaN	NaN	-3.2	-6.7
187.0	13553	3.4700	0.0216	NaN	NaN

Depth (mm from top)	Age (Years BP)	Mg/Ca (mmol/mol)	Sr/Ca (mmol/mol)	d18O (‰, V-PDB)	d13C (‰, V-PDB)
187.5	13623	NaN	NaN	-3.51	-6.48
188.0	13692	3.8800	0.0224	NaN	NaN
188.5	13761	NaN	NaN	-3.15	-6.57
189.0	13828	3.8700	0.0285	NaN	NaN
189.5	13894	NaN	NaN	-2.9	-6.47
190.5	14016	4.0304	0.0251	-3.3	-5.39
191.0	14074	3.8072	0.0265	NaN	NaN
191.5	14128	NaN	NaN	-2.5	-5.51
192.5	14221	3.8600	0.0314	NaN	NaN
193.0	14260	NaN	NaN	-2.75	-5.23
193.5	14296	NaN	NaN	-3.56	-5.5
194.0	14330	NaN	NaN	-3.52	-5.1
194.5	14363	3.5171	0.0280	NaN	NaN
195.0	14395	3.4900	0.0272	-3.03	-5.92
196.0	14456	3.6100	0.0285	-3.4	-5.28
197.0	14512	3.5300	0.0277	-2.85	-5.18
198.0	14564	3.8700	0.0312	-2.49	-4.28
199.0	14614	4.0000	0.0340	-2.51	-4.48
200.0	14659	4.5600	0.0350	-2.7	-3.81
201.0	14703	4.4500	0.0311	-2.51	-3.56
202.0	14747	4.3000	0.0281	-2.85	-3.66
203.0	14786	4.5600	0.0308	-3.27	-3.34
204.0	14827	5.0600	0.0308	-3.26	-3.59
205.0	14867	4.7900	0.0293	-3.76	-3.19
206.0	14909	4.5700	0.0280	-3.95	-3.41
207.0	14952	4.8000	0.0274	-3.53	-2.94
208.0	14996	4.5800	0.0325	-4.14	-3.42
209.0	15044	4.5800	0.0322	-3.43	-3.35
210.0	15092	4.7400	0.0306	-3.67	-3.78

Depth (mm from top)	Age (Years BP)	Mg/Ca (mmol/mol)	Sr/Ca (mmol/mol)	d18O (‰, V-PDB)	d13C (‰, V-PDB)
211.0	15145	4.6400	0.0286	-3.58	-3.36
212.0	15200	4.6600	0.0254	-3.36	-2.58
213.0	15261	4.9600	0.0262	-3.53	-2.62
214.0	15326	5.1100	0.0269	-3.45	-2.37
215.0	15398	5.2300	0.0285	-3.07	-3.07
216.0	15474	5.5100	0.0325	-3.32	-2.76
217.0	15556	5.6000	0.0296	-2.9	-2.14
218.0	15643	6.1500	0.0323	-2.88	-1.57
219.0	15730	5.8400	0.0315	-2.83	-2.99
219.0	15730	NaN	NaN	NaN	NaN
219.5	15772	5.3164	0.0346	NaN	NaN
220.0	15817	5.5598	0.0317	NaN	NaN
221.0	15905	NaN	NaN	-3.56	-3.7
221.5	15947	4.8513	0.0277	NaN	NaN
222.0	15991	NaN	NaN	-2.79	-3.56
222.5	16035	NaN	NaN	-3.28	-3.25
223.0	16080	7.5504	0.0338	NaN	NaN
224.5	16206	NaN	NaN	-2.05	-2.36
225.0	16247	4.2500	0.0249	-1.72	-2.72
225.5	16288	4.2796	0.0227	NaN	NaN
226.0	16328	4.1600	0.0254	-1.64	-4.4
227.0	16406	3.7100	0.0248	-1.62	-5
228.0	16478	4.1400	0.0253	-1.07	-3.03
229.0	16548	3.5900	0.0258	-1.44	-4.84
230.0	16610	3.6400	0.0236	-2.27	-5.05
231.0	16666	3.5200	0.0226	NaN	NaN
232.0	16716	4.0600	0.0272	-1.34	-4.25
233.0	16759	4.2300	0.0270	-0.93	-3.99
234.0	16801	4.6700	0.0278	-1.48	-3.74

Depth (mm from top)	Age (Years BP)	Mg/Ca (mmol/mol)	Sr/Ca (mmol/mol)	d18O (‰, V-PDB)	d13C (‰, V-PDB)
235.0	16842	4.0700	0.0288	-1.57	-3.61
236.0	16882	4.8700	0.0270	-1.56	-2.7
237.0	16928	4.5100	0.0262	-1.62	-3.54
238.0	16979	3.6700	0.0242	-1.5	-5.2
239.0	17040	3.9200	0.0263	-1.72	-4.58
240.0	17112	4.7100	0.0294	-2.12	-3.2
241.0	17200	4.4800	0.0282	-1.7	-2.56
242.0	17309	3.9100	0.0281	-1.79	-3.12
243.0	17435	4.0500	0.0290	-1.81	-2.36
244.0	17582	4.4600	0.0275	NaN	NaN
245.0	17746	4.6500	0.0270	-1.68	-1.26
246.0	17921	4.4900	0.0279	-1.34	-0.47
247.0	18104	4.2900	0.0267	-1.37	-1
248.0	18294	4.0900	0.0276	-1.29	-2.07
249.0	18490	4.1300	0.0265	-1.72	-2.46
250.0	18689	4.1500	0.0246	-1.39	-2.36
251.0	18891	4.3900	0.0242	-1.24	-1.71
252.0	19098	4.2600	0.0237	-1.26	-1.83
253.0	19295	3.3500	0.0222	-1.49	-3.15
254.0	19484	3.1300	0.0210	-1.75	-3.59
255.0	19667	3.0100	0.0222	-1.71	-4.11
256.0	19839	3.1500	0.0266	-2.2	-4.22
257.0	19997	3.3500	0.0222	-2.14	-3.65
258.0	20147	3.2800	0.0216	-1.89	-3.78
259.0	20295	3.1500	0.0233	-1.99	-4.14
260.0	20441	3.0500	0.0212	-2.2	-4.28
261.0	20583	3.2500	0.0218	-2.32	-3.15
262.0	20725	3.5400	0.0226	-2.4	-2.21
263.0	20864	3.9200	0.0224	-2.98	-1.42

Depth (mm from top)	Age (Years BP)	Mg/Ca (mmol/mol)	Sr/Ca (mmol/mol)	d18O (‰, V-PDB)	d13C (‰, V-PDB)
264.0	21001	3.4900	0.0221	-2.65	-2.32
265.0	21134	3.4400	0.0237	-3.06	-2.18
266.0	21268	3.3900	0.0203	-2.6	-2.45
267.0	21397	3.7500	0.0206	-2.81	-1.46
268.0	21523	3.7400	0.0211	-3.04	-1.92
269.0	21650	3.5500	0.0228	-3.18	-1.91
270.0	21771	3.5200	0.0179	-3.03	-2.77

Appendix B

Appendix B. Figures

Appendix Figure 1. Investigation of the precipitation dipole between northern and southern Mesoamerica across the Last Deglaciation. From North to South: GC1 Mg/Ca record (this work); Lake Chalco Ti % (Lozano-Garcia et al. 2015); Juxtlahuaca Cave δ18O (Lachniet et al. 2015). A "wet" signal is indicated up along the y-axis and a "dry" signal is indicated down along the y-axis. The Santa Isabel Ixtapan paleolithic archaeology site (dating to 13 ka) is noted with a white star.

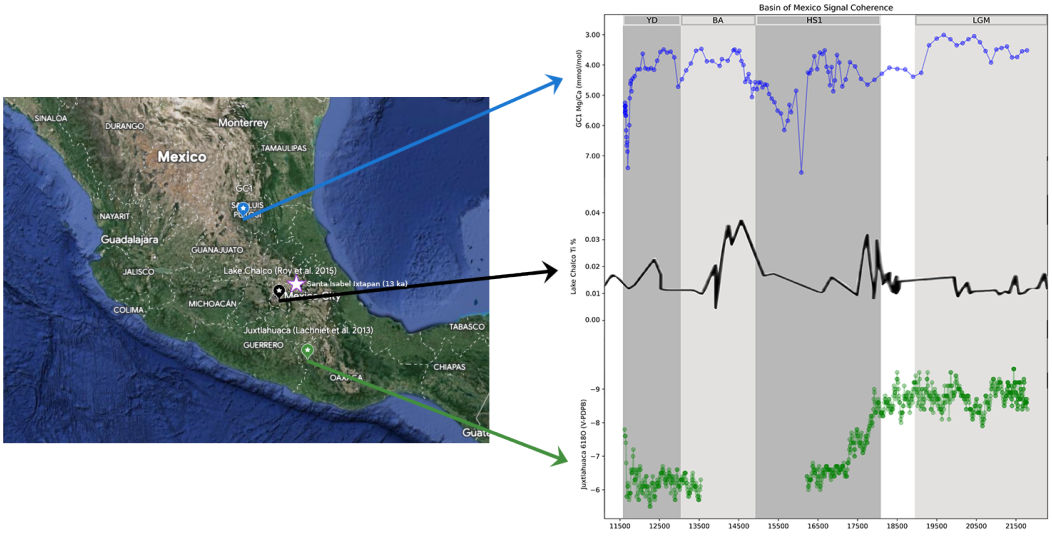

Appendix C

Bibliography

Ardelean, C. F., Becerra-Valdivia, L., Pedersen, M. W., Schwenninger, J.-L., Oviatt, C. G., Macías-Quintero, J. I., Arroyo-Cabrales, J., Sikora, M., Ocampo-Díaz, Y. Z. E., Rubio-Cisneros, I. I., Watling, J. G., de Medeiros, V. B., De Oliveira, P. E., Barba-Pingarón, L., Ortiz-Butrón, A., Blancas-Vázquez, J., Rivera-González, I., Solís-Rosales, C., Rodríguez-Ceja, M., … Willerslev, E. (2020). Evidence of human occupation in Mexico around the Last Glacial Maximum. *Nature*, *584*(7819), Article 7819. https://doi.org/10.1038/s41586-020-2509-0

Arienzo, M. M., Swart, P. K., Pourmand, A., Broad, K., Clement, A. C., Murphy, L. N., Vonhof, H. B., \& Kakuk, B. (2015). Bahamian speleothem reveals temperature decrease associated with Heinrich stadials. *Earth and Planetary Science Letters*, *430*, 377–386. https://doi.org/10.1016/j.epsl.2015.08.035

Ayalon, A., Bar-Matthews, M., \& Sass, E. (1998). Rainfall-recharge relationships within a karstic terrain in the Eastern Mediterranean semi-arid region, Israel: δ 18O and δD characteristics. *Journal of Hydrology*, *207*(1), 18–31. https://doi.org/10.1016/S0022-1694(98)00119-X

Baker, A., Hartmann, A., Duan, W., Hankin, S., Comas-Bru, L., Cuthbert, M. O., Treble, P. C., Banner, J., Genty, D., Baldini, L. M., Bartolomé, M., Moreno, A., Pérez-Mejías, C., \& Werner, M. (2019). Global analysis reveals climatic controls on the oxygen isotope composition of cave drip water. *Nature Communications*, *10*(1), Article 1. https://doi.org/10.1038/s41467-019-11027-w

Balco, G., \& Rovey, C. W., II. (2010). Absolute chronology for major Pleistocene advances of the Laurentide Ice Sheet. *Geology*, *38*(9), 795–798. https://doi.org/10.1130/G30946.1

Bennett, M. R., Bustos, D., Pigati, J. S., Springer, K. B., Urban, T. M., Holliday, V. T., Reynolds, S. C., Budka, M., Honke, J. S., Hudson, A. M., Fenerty, B., Connelly, C., Martinez, P. J., Santucci, V. L., \& Odess, D. (2021). Evidence of humans in North America during the Last Glacial Maximum. *Science*, *373*(6562), 1528–1531. https://doi.org/10.1126/science.abg7586

Bhattacharya, T., Tierney, J. E., \& DiNezio, P. (2017). Glacial reduction of the North American Monsoon via surface cooling and atmospheric ventilation. *Geophysical Research Letters*, *44*(10), 5113–5122. https://doi.org/10.1002/2017GL073632

Bhattacharya, T., \& Coats, S. (2020). Atlantic-Pacific Gradients Drive Last Millennium Hydroclimate Variability in Mesoamerica. *Geophysical Research Letters*, *47*(13), e2020GL088061. https://doi.org/10.1029/2020GL088061

Braje, T. J., Dillehay, T. D., Erlandson, J. M., Klein, R. G., \& Rick, T. C. (2017). Finding the first Americans. *Science*, *358*(6363), 592–594. https://doi.org/10.1126/science.aao5473

Breitenbach, S. F., Rehfeld, K., Goswami, B., Baldini, J. U., Ridley, H. E., Kennett, D. J., ... \& Marwan, N. (2012). Constructing proxy records from age models (COPRA). *Climate of the Past*, *8*(5), 1765-1779.

Broecker, W., Bond, G., Klas, M., Clark, E., \& McManus, J. (1992). Origin of the northern

Atlantic's Heinrich events. *Climate Dynamics*, *6*(3), 265–273. https://doi.org/10.1007/BF00193540

Bush, M. B., Correa-metrio, A. Y., Hodell, D. A., Brenner, M., Anselmetti, F. S., Ariztegui, D., Mueller, A. D., Curtis, J. H., Grzesik, D. A., Burton, C., \& Gilli, A. (2009). Re-evaluation of Climate Change in Lowland Central America During the Last Glacial Maximum Using New Sediment Cores from Lake Petén Itzá, Guatemala. In F. Vimeux, F. Sylvestre, \& M. Khodri (Eds.), *Past Climate Variability in South America and Surrounding Regions: From the Last Glacial Maximum to the Holocene* (pp. 113–128). Springer Netherlands. https://doi.org/10.1007/978-90-481-2672-9_5

Chevalier, M., Brewer, S., \& Chase, B. M. (2017). Qualitative assessment of PMIP3 rainfall simulations across the eastern African monsoon domains during the mid-Holocene and the Last Glacial Maximum. Quaternary Science Reviews, 156, 107–120.https://doi.org/10.1016/j.quascirev.2016.11.028

Cook, K. H., \& Vizy, E. K. (2010). Hydrodynamics of the Caribbean Low-Level Jet and Its Relationship to Precipitation. *Journal of Climate*, *23*(6), 1477–1494. https://doi.org/10.1175/2009JCLI3210.1

Cruz, F. W., Burns, S. J., Jercinovic, M., Karmann, I., Sharp, W. D., \& Vuille, M. (2007). Evidence of rainfall variations in Southern Brazil from trace element ratios (Mg/Ca and Sr/Ca) in a Late Pleistocene stalagmite. *Geochimica et Cosmochimica Acta*, *71*(9), 2250–2263. https://doi.org/10.1016/j.gca.2007.02.005

Davis, L. G., \& Madsen, D. B. (2020). The coastal migration theory: Formulation and testable hypotheses. *Quaternary Science Reviews*, *249*, 106605. https://doi.org/10.1016/j.quascirev.2020.106605

Day, C. C., \& Henderson, G. M. (2013). Controls on trace-element partitioning in cave-analogue calcite. *Geochimica et Cosmochimica Acta*, *120*, 612–627. https://doi.org/10.1016/j.gca.2013.05.044

Dillehay, Tom. (2000). The Settlement of the Americas: A New Prehistory. Basic Books, New York.

Dillehay, T. D., Ocampo, C., Saavedra, J., Sawakuchi, A. O., Vega, R. M., Pino, M., Collins, M. B., Cummings, L. S., Arregui, I., Villagran, X. S., Hartmann, G. A., Mella, M., González, A., \& Dix, G. (2015). New Archaeological Evidence for an Early Human Presence at Monte Verde, Chile. *PLOS ONE*, *10*(11), e0141923. https://doi.org/10.1371/journal.pone.0141923

Erlandson, J. M., Graham, M. H., Bourque, B. J., Corbett, D., Estes, J. A., \& Steneck, R. S. (2007). The Kelp Highway Hypothesis: Marine Ecology, the Coastal Migration Theory, and the Peopling of the Americas. *The Journal of Island and Coastal Archaeology*, *2*(2), 161–174. https://doi.org/10.1080/15564890701628612

Fairchild, I. J., Borsato, A., Tooth, A. F., Frisia, S., Hawkesworth, C. J., Huang, Y., McDermott, F., \& Spiro, B. (2000). Controls on trace element (Sr–Mg) compositions

of carbonate cave waters: Implications for speleothem climatic records. *Chemical Geology*, *166*(3), 255–269. https://doi.org/10.1016/S0009-2541(99)00216-8

Fairchild, I. J., Smith, C. L., Baker, A., Fuller, L., Spötl, C., Mattey, D., McDermott, F., \& E.i.m.f. (2006). Modification and preservation of environmental signals in speleothems. *Earth-Science Reviews*, *75*(1), 105–153. https://doi.org/10.1016/j.earscirev.2005.08.003

Fairchild, Ian John and Emily Anne McMillan. 2007. Speleothems as indicators of wet and dry periods. International Journal of Speleology, 36: 69-74.

Gonzalez, S., \& Huddart, D. (n.d.). *The Late Pleistocene Human Occupation of Mexico*.

Gowan, E. J., Tregoning, P., Purcell, A., Montillet, J.-P., \& McClusky, S. (2016). A model of the western Laurentide Ice Sheet, using observations of glacial isostatic adjustment. *Quaternary Science Reviews*, *139*, 1–16. https://doi.org/10.1016/j.quascirev.2016.03.003

Griffiths, M. L., Drysdale, R. N., Vonhof, H. B., Gagan, M. K., Zhao, J., Ayliffe, L. K., Hantoro, W. S., Hellstrom, J. C., Cartwright, I., Frisia, S., \& Suwargadi, B. W. (2010). Younger Dryas–Holocene temperature and rainfall history of southern Indonesia from δ18O in speleothem calcite and fluid inclusions. *Earth and Planetary Science Letters*, *295*(1), 30–36. https://doi.org/10.1016/j.epsl.2010.03.018

Groucutt, H. S., Petraglia, M. D., Bailey, G., Scerri, E. M. L., Parton, A., Clark-Balzan, L., Jennings, R. P., Lewis, L., Blinkhorn, J., Drake, N. A., Breeze, P. S., Inglis, R. H., Devès, M. H., Meredith-Williams, M., Boivin, N., Thomas, M. G., \& Scally, A. (2015). Rethinking the dispersal of Homo sapiens out of Africa. *Evolutionary Anthropology: Issues, News, and Reviews*, *24*(4), 149–164. https://doi.org/10.1002/evan.21455

He, C., Liu, Z., Otto-Bliesner, B. L., Brady, E. C., Zhu, C., Tomas, R., Buizert, C., \& Severinghaus, J. P. (2021). Abrupt Heinrich Stadial 1 cooling missing in Greenland oxygen isotopes. *Science Advances*, *7*(25), eabh1007. https://doi.org/10.1126/sciadv.abh1007

Hodell, D. A., Anselmetti, F. S., Ariztegui, D., Brenner, M., Curtis, J. H., Gilli, A., Grzesik, D. A., Guilderson, T. J., Müller, A. D., Bush, M. B., Correa-Metrio, A., Escobar, J., \& Kutterolf, S. (2008). An 85-ka record of climate change in lowland Central America. *Quaternary Science Reviews*, *27*(11), 1152–1165. https://doi.org/10.1016/j.quascirev.2008.02.008

Hulbe, C. L., MacAyeal, D. R., Denton, G. H., Kleman, J., \& Lowell, T. V. (2004). Catastrophic ice shelf breakup as the source of Heinrich event icebergs. *Paleoceanography*, *19*(1). https://doi.org/10.1029/2003PA000890

Johnson, K. R., Hu, C., Belshaw, N. S., \& Henderson, G. M. (2006). Seasonal trace-element and stable-isotope variations in a Chinese speleothem: The potential for high-resolution paleomonsoon reconstruction. *Earth and Planetary Science Letters*, *244*(1), 394–407. https://doi.org/10.1016/j.epsl.2006.01.064

Köhler, P., Knorr, G., Buiron, D., Lourantou, A., \& Chappellaz, J. (2011). Abrupt rise in atmospheric CO_2 at the onset of the Bølling/Allerød: In-situ ice core data versus true

atmospheric signals. *Climate of the Past*, *7*(2), 473–486. https://doi.org/10.5194/cp-7-473-2011

Lachniet, M. S., \& Vazquez-Selem, L. (2005). Last Glacial Maximum equilibrium line altitudes in the circum-Caribbean (Mexico, Guatemala, Costa Rica, Colombia, and Venezuela). *Quaternary International*, *138–139*, 129–144. https://doi.org/10.1016/j.quaint.2005.02.010

Lea, D. W., Pak, D. K., Peterson, L. C., \& Hughen, K. A. (2003). Synchroneity of Tropical and High-Latitude Atlantic Temperatures over the Last Glacial Termination. *Science*, *301*(5638), 1361–1364. https://doi.org/10.1126/science.1088470

Llamas, B., Fehren-Schmitz, L., Valverde, G., Soubrier, J., Mallick, S., Rohland, N., Nordenfelt, S., Valdiosera, C., Richards, S. M., Rohrlach, A., Romero, M. I. B., Espinoza, I. F., Cagigao, E. T., Jiménez, L. W., Makowski, K., Reyna, I. S. L., Lory, J. M., Torrez, J. A. B., Rivera, M. A., … Haak, W. (2016). Ancient mitochondrial DNA provides high-resolution time scale of the peopling of the Americas. *Science Advances*, *2*(4), e1501385. https://doi.org/10.1126/sciadv.1501385

Lozano-García, S., Ortega, B., Roy, P. D., Beramendi-Orosco, L., \& Caballero, M. (2015). Climatic variability in the northern sector of the American tropics since the latest MIS 3. *Quaternary Research*, *84*(2), 262–271. https://doi.org/10.1016/j.yqres.2015.07.002

Maldonado, T., Rutgersson, A., Caballero, R., Pausata, F. S. R., Alfaro, E., \& Amador, J. (2017). The role of the meridional sea surface temperature gradient in controlling the Caribbean low-level jet. *Journal of Geophysical Research: Atmospheres*, *122*(11), 5903–5916. https://doi.org/10.1002/2016JD026025

Martinez, S., Delgado, J., Escolero, O., Domínguez, E., Suarez, M., Fernandez-Bernal, A., \& De La Rosa, M. A. (2010). Socio-economic development in arid zones: the influence of water availability in the San Luis Potosi Basin, Mexico. *Arid environmental. Nova, New York*.

Max, L., Nürnberg, D., Chiessi, C. M., Lenz, M. M., \& Mulitza, S. (2022). Subsurface ocean warming preceded Heinrich Events. *Nature Communications*, *13*(1), Article 1. https://doi.org/10.1038/s41467-022-31754-x

McManus, J. F., Francois, R., Gherardi, J. M., Keigwin, L. D., \& Brown-Leger, S. (2004). Collapse and rapid resumption of Atlantic meridional circulation linked to deglacial climate changes. *nature*, *428*(6985), 834-837.

McMillan, E. A., Fairchild, I. J., Frisia, S., Borsato, A., \& McDermott, F. (2005). Annual trace element cycles in calcite–aragonite speleothems: Evidence of drought in the western Mediterranean 1200–1100 yr BP. *Journal of Quaternary Science*, *20*(5), 423–433. https://doi.org/10.1002/jqs.943

Meltzer, D. J. (2003). Peopling of North America. In *The Quaternary Period in the United States* (Vol. 1, pp. 539–563). Elsevier. https://doi.org/10.1016/S1571-0866(03)01026-1

Miller, N., Banner, J., Feng, W., Gonzales, A., \& Kozdon, R. (2021). Hydroclimate response in Texas and Gulf of Mexico to rapid warming during the last deglacial:

High-resolution speleothem proxy and monitoring evidence. *Quaternary Science Reviews*, *273*, 107244. https://doi.org/10.1016/j.quascirev.2021.107244

Acosta-Ochoa, G., De Tapia, E. M., \& Arroyo-Cabrales, J. (2021). The Lacustrine Preceramic Cultures in the Basin of Mexico. In J. C. Lohse, A. Borejsza, \& A. A. Joyce (Eds.), *Preceramic Mesoamerica* (1st ed., pp. 278–303). Routledge. https://doi.org/10.4324/9780429054679-9

Osman, M. B., Tierney, J. E., Zhu, J., Tardif, R., Hakim, G. J., King, J., \& Poulsen, C. J. (2021). Globally resolved surface temperatures since the Last Glacial Maximum. *Nature*, *599*(7884), 239-244.

Partin, J. W., Quinn, T. M., Shen, C.-C., Okumura, Y., Cardenas, M. B., Siringan, F. P., Banner, J. L., Lin, K., Hu, H.-M., \& Taylor, F. W. (2015). Gradual onset and recovery of the Younger Dryas abrupt climate event in the tropics. *Nature Communications*, *6*(1), Article 1. https://doi.org/10.1038/ncomms9061

Petraglia, M. D., Groucutt, H. S., Guagnin, M., Breeze, P. S., \& Boivin, N. (2020). Human responses to climate and ecosystem change in ancient Arabia. *Proceedings of the National Academy of Sciences*, *117*(15), 8263–8270. https://doi.org/10.1073/pnas.1920211117

Pico, T., Creveling, J. R., \& Mitrovica, J. X. (2017). Sea-level records from the U.S. mid-Atlantic constrain Laurentide Ice Sheet extent during Marine Isotope Stage 3. *Nature Communications*, *8*(1), Article 1. https://doi.org/10.1038/ncomms15612

Potter, B. A., Beaudoin, A. B., Haynes, C. V., Holliday, V. T., Holmes, C. E., Ives, J. W., Kelly, R., Llamas, B., Malhi, R., Miller, S., Reich, D., Reuther, J. D., Schiffels, S., \& Surovell, T. (2018). Arrival routes of first Americans uncertain. *Science*, *359*(6381), 1224–1225. https://doi.org/10.1126/science.aar8233

Raff, J. A., \& Bolnick, D. A. (2014). Genetic roots of the first Americans. *Nature*, *506*(7487), Article 7487. https://doi.org/10.1038/506162

Rauscher, S. A., Kucharski, F., \& Enfield, D. B. (2010). The role of regional SST warming variations in the drying of Meso-America in future climate projections. *AGU Fall Meeting Abstracts*, *2010*, GC21D-07.

Raynaud, D., Barnola, J.-M., Chappellaz, J., Blunier, T., Indermühle, A., \& Stauffer, B. (2000). The ice record of greenhouse gases: A view in the context of future changes. *Quaternary Science Reviews*, *19*(1), 9–17. https://doi.org/10.1016/S0277-3791(99)00082-7

Renssen, H., Goosse, H., Roche, D. M., \& Seppä, H. (2018). The global hydroclimate response during the Younger Dryas event. *Quaternary Science Reviews*, *193*, 84–97. https://doi.org/10.1016/j.quascirev.2018.05.033

Roy, P. D., Rivero-Navarrete, A., Sánchez-Zavala, J. L., Beramendi-Orosco, L. E., Muthu-Sankar, G., \& Lozano-Santacruz, R. (2016). Atlantic Ocean modulated hydroclimate of the subtropical northeastern Mexico since the last glacial maximum

and comparison with the southern US. *Earth and Planetary Science Letters*, *434*, 141–150. https://doi.org/10.1016/j.epsl.2015.11.048

Roy, P. D., Vera-Vera, G., Curtis, J. H., Sánchez-Zavala, J. L., Quiroz-Jiménez, J. D., \& Muthu Sankar, G. (2019). Response of arid northeast Mexico to global climate changes during the late Pleistocene to the middle Holocene. *Earth Surface Processes and Landforms*, *44*(11), 2211–2222. https://doi.org/10.1002/esp.4645

Roy, P. D., Vera-Vera, G., Sánchez-Zavala, J. L., Shanahan, T. M., Quiroz-Jiménez, J. D., Curtis, J. H., Girón-García, P., Lemus-Neri, V. H., \& Muthusankar, G. (2020). Depositional histories of vegetation and rainfall intensity in Sierra Madre Oriental Mountains (northeast Mexico) since the late Last Glacial. *Global and Planetary Change*, *187*, 103136. https://doi.org/10.1016/j.gloplacha.2020.103136

Scheff, J., Seager, R., Liu, H., \& Coats, S. (2017). Are Glacials Dry? Consequences for Paleoclimatology and for Greenhouse Warming. *Journal of Climate*, *30*(17), 6593–6609. https://doi.org/10.1175/JCLI-D-16-0854.1

Sear, D. A., Allen, M. S., Hassall, J. D., Maloney, A. E., Langdon, P. G., Morrison, A. E., Henderson, A. C. G., Mackay, H., Croudace, I. W., Clarke, C., Sachs, J. P., Macdonald, G., Chiverrell, R. C., Leng, M. J., Cisneros-Dozal, L. M., Fonville, T., \& Pearson, E. (2020). Human settlement of East Polynesia earlier, incremental, and coincident with prolonged South Pacific drought. *Proceedings of the National Academy of Sciences*, *117*(16), 8813–8819. https://doi.org/10.1073/pnas.1920975117

Serrato Marks, G., Medina-Elizalde, M., Burns, S., Weldeab, S., Lases-Hernandez, F., Cazares, G., \& McGee, D. (2021). Evidence for Decreased Precipitation Variability in the Yucatán Peninsula During the Mid-Holocene. *Paleoceanography and Paleoclimatology*, *36*(5), e2021PA004219. https://doi.org/10.1029/2021PA004219

Sinclair, D. J. (2011). Two mathematical models of Mg and Sr partitioning into solution during incongruent calcite dissolution: Implications for dripwater and speleothem studies. *Chemical Geology*, *283*(3), 119–133. https://doi.org/10.1016/j.chemgeo.2010.05.022

Su, Z., Ingersoll, A. P., \& He, F. (2016). On the Abruptness of Bølling–Allerød Warming. *Journal of Climate*, *29*(13), 4965–4975. https://doi.org/10.1175/JCLI-D-15-0675.1

Treble, P. C., Fairchild, I. J., Griffiths, A., Baker, A., Meredith, K. T., Wood, A., \& McGuire, E. (2015). Impacts of cave air ventilation and in-cave prior calcite precipitation on Golgotha Cave dripwater chemistry, southwest Australia. *Quaternary Science Reviews*, *127*, 61–72. https://doi.org/10.1016/j.quascirev.2015.06.001

Wang, C., \& Fiedler, P. C. (2006). ENSO variability and the eastern tropical Pacific: A review. *Progress in Oceanography*, *69*(2), 239–266. https://doi.org/10.1016/j.pocean.2006.03.004

Waters, M. R., \& Stafford, T. W. (2007). Redefining the Age of Clovis: Implications for the Peopling of the Americas. *Science*, *315*(5815), 1122–1126. https://doi.org/10.1126/science.1137166

Williams, T. J., Collins, M. B., Rodrigues, K., Rink, W. J., Velchoff, N., Keen-Zebert, A., Gilmer, A., Frederick, C. D., Ayala, S. J., \& Prewitt, E. R. (2018). Evidence of an early projectile point technology in North America at the Gault Site, Texas, USA. *Science Advances*, *4*(7), eaar5954. https://doi.org/10.1126/sciadv.aar5954

Wright, K. T., Johnson, K. R., Bhattacharya, T., Marks, G. S., McGee, D., Elsbury, D., Peings, Y., Lacaille-Muzquiz, J.-L., Lum, G., Beramendi-Orosco, L., \& Magnusdottir, G. (2022). Precipitation in Northeast Mexico Primarily Controlled by the Relative Warming of Atlantic SSTs. *Geophysical Research Letters*, *49*(11), e2022GL098186. https://doi.org/10.1029/2022GL098186

Yang, H., Krebs-Kanzow, U., Kleiner, T., Sidorenko, D., Rodehacke, C. B., Shi, X., Gierz, P., Niu, L., Gowan, E. J., Hinck, S., Liu, X., Stap, L. B., \& Lohmann, G. (2022). Impact of paleoclimate on present and future evolution of the Greenland Ice Sheet. *PLOS ONE*, *17*(1), e0259816. https://doi.org/10.1371/journal.pone.0259816